NAADP and the two-pore channel protein 1 participate in the acrosome reaction in mammalian spermatozoa

Lilli Arndt[a], Jan Castonguay[b], Elisabeth Arlt[a], Dorke Meyer[a], Sami Hassan[c], Heike Borth[a], Susanna Zierler[a], Gunther Wennemuth[d], Andreas Breit[a], Martin Biel[c], Christian Wahl-Schott[c], Thomas Gudermann[a], Norbert Klugbauer[b], and Ingrid Boekhoff[a]

[a]Walther Straub Institute of Pharmacology and Toxicology and [c]Department of Pharmacy, Ludwig-Maximilians University, 81377 München, Germany; [b]Institute for Experimental and Clinical Pharmacology and Toxicology, Albert-Ludwigs-University, 79104 Freiburg, Germany; [d]Institute for Anatomy, University of Duisburg-Essen, 45141 Essen, Germany

ABSTRACT **The functional relationship between the formation of hundreds of fusion pores during the acrosome reaction in spermatozoa and the mobilization of calcium from the acrosome has been determined only partially. Hence, the second messenger NAADP, promoting efflux of calcium from lysosome-like compartments and one of its potential molecular targets, the two-pore channel 1 (TPC1), were analyzed for its involvement in triggering the acrosome reaction using a TPCN1 gene–deficient mouse strain. The present study documents that TPC1 and NAADP-binding sites showed a colocalization at the acrosomal region and that treatment of spermatozoa with NAADP resulted in a loss of the acrosomal vesicle that showed typical properties described for TPCs: Registered responses were not detectable for its chemical analogue NADP and were blocked by the NAADP antagonist *trans*-Ned-19. In addition, two narrow bell-shaped dose-response curves were identified with maxima in either the nanomolar or low micromolar NAADP concentration range, where TPC1 was found to be responsible for activating the low affinity pathway. Our finding that two convergent NAADP-dependent pathways are operative in driving acrosomal exocytosis supports the concept that both NAADP-gated cascades match local NAADP concentrations with the efflux of acrosomal calcium, thereby ensuring complete fusion of the large acrosomal vesicle.**

Monitoring Editor
Julie Brill
The Hospital for Sick Children

Received: Sep 10, 2013
Revised: Jan 13, 2014
Accepted: Jan 15, 2014

INTRODUCTION

Sperm contain a large, Golgi-derived secretory vesicle—the acrosome—located above the anterior part of the sperm nucleus. The acrosome is characterized by unique properties, all essential to ensure successful fertilization. It contains hydrolytic enzymes that allow sperm to break down the extracellular glycoprotein matrix surrounding the egg (for review see Florman *et al.*, 2008; Wassarman and Litscher, 2008; Visconti *et al.*, 2011). The release of digestive enzymes, called the acrosome reaction, is accomplished by Ca^{2+}-regulated exocytosis (for review see Mayorga *et al.*, 2007; Tomes, 2007), a highly conserved mechanism controlling membrane- trafficking processes in different cell types (for reviews see Jahn and Fasshauer, 2012; Rizo and Sudhof, 2012). In addition, the acrosome also acts as an intracellular Ca^{2+} store in mammalian spermatozoa (De Blas *et al.*, 2002; Herrick *et al.*, 2005; Costello *et al.*, 2009), the luminal pH of which was found to be strongly acidic (pH 5.3; Meizel and Deamer, 1978; Nakanishi *et al.*, 2001). Owing to its parallels to the endolysosomal system (for review see Dell'Angelica *et al.*, 2000), such as the ability to store digestive enzymes, as well as to function as an intracellular Ca^{2+} store (Patel and Docampo, 2010), the

This article was published online ahead of print in MBoC in Press (http://www.molbiolcell.org/cgi/doi/10.1091/mbc.E13-09-0523) on January 22, 2014.

Address correspondence to: Ingrid Boekhoff (ingrid.boekhoff@lrz.uni-muenchen.de).

Abbreviations used: 2-APB, 2-aminoethyldiphenyl borate; $[Ca^{2+}]_i$, intracellular calcium concentration; CICR, Ca^{2+}-induced Ca^{2+} release; FITC, fluorescein isothiocyanate; IP_3-R, inositol 1,4,5-trisphosphate receptor; NAADP, nicotinic acid adenine dinucleotide phosphate; NAADP-AM, NAADP acetoxymethyl ester; NADP, nicotinamide adenine dinucleotide phosphate; NPC1, Niemann–Pick type C1; P_2, crude membrane pellet; PNA, peanut agglutinin; Rab3A, Ras-like guanine nucleotide–binding protein; RR, ruthenium red; RyR, ryanodine receptor; SLO, streptolysine O; TPC, two-pore channel.

acrosomal vesicle has been referred to as a lysosome-related organelle (Hartree, 1975).

The intracellular messenger nicotinic acid adenine dinucleotide phosphate (NAADP) is crucial for Ca^{2+} mobilization in morphologically very diverse acidic organelles, such as acidocalcisomes, vacuoles, endosomes, lysosomes, lysosome-like acidic compartments, the Golgi complex, and secretory granules (Patel and Docampo, 2010; Zhu *et al.*, 2010a; Hooper and Patel, 2012). Although the mechanism/s of NAADP synthesis are unclear (Patel *et al.*, 2011; Schmid *et al.*, 2011; Galione and Chuang, 2012), the search for NAADP receptors resulted in the identification of endolysosomal cation channels termed two-pore channels (TPCs; Brailoiu *et al.*, 2009; Calcraft *et al.*, 2009; Zong *et al.*, 2009). The three members of the TPC channel family share the same membrane topology, composed of two homologous domains each containing six transmembrane segments and two pore loops (Yu *et al.*, 2005; Zong *et al.*, 2009; Zhu *et al.*, 2010a). Whereas the *TPCN3* gene is a pseudogene in primates, TPC1 and TPC2 are present in most mammals, including humans, rats, and mice (Calcraft *et al.*, 2009; Brailoiu *et al.*, 2010).

Although it is not clear whether NAADP directly binds to TPC channel proteins (Guse, 2012; Lin-Moshier *et al.*, 2012; Walseth *et al.*, 2012) and whether TPCs can also be activated by phosphatidylinositol 3,5-bisphosphate (Wang *et al.*, 2012), TPCs display basic properties observed for NAADP-induced intracellular Ca^{2+} mobilization: dose–response curves of NAADP-triggered Ca^{2+} efflux from acidic stores are typically bell shaped with a peak in the submillimolar concentration range (Zong *et al.*, 2009; Galione, 2011; Guse, 2012). In addition, TPCs enter a desensitized state upon pretreatment with very low, subthreshold concentrations of NAADP (Aarhus *et al.*, 1996; Genazzani *et al.*, 1996; Cancela *et al.*, 1999; Zong *et al.*, 2009; Zhu *et al.*, 2010c). Furthermore, TPC-triggered Ca^{2+} release is almost completely absent in lysosomes treated with bafilomycin (for review see Zhu *et al.*, 2010c); bafilomycin is a vacuolar H^+-ATPase inhibitor that disrupts the acid luminal pH of organelles (Bowman *et al.*, 1988) and thus their ability to store Ca^{2+}. Of importance, mobilization of Ca^{2+} by TPCs is amplified by increasing the susceptibility of 1,4,5-inositol trisphosphate receptors (IP_3-Rs) and ryanodine receptors (RyRs). This points toward a Ca^{2+}-induced Ca^{2+} release (CICR) reaction of TPCs (Cancela *et al.*, 1999; Galione *et al.*, 2009; Zhu *et al.*, 2010a). The CICR is a quite common positive feedback signaling process that converts spatially restricted Ca^{2+} signals into more global Ca^{2+} waves (Berridge, 2002; Rahman and Taylor, 2009; Zhu *et al.*, 2010a).

The observation that the acrosomal vesicle regulates its own exocytosis by acting as a lysosome-related Ca^{2+} reservoir (De Blas *et al.*, 2002; Herrick *et al.*, 2005) indicates a considerable effect of intracellular Ca^{2+} channels on regulated membrane fusion processes. This concept was recently also described for lytic granules of cytotoxic T lymphocytes (Davis *et al.*, 2012). However, our knowledge about the molecular identity and functional role of ion channels controlling Ca^{2+} efflux from intracellular storage sites in sperm is very limited (Costello *et al.*, 2009; Darszon *et al.*, 2011). Among the archetypal intracellular Ca^{2+}-release channels located in sarcoplasmic/endoplasmic reticulum membranes, the IP_3-R (Walensky and Snyder, 1995; Kuroda *et al.*, 1999; Ho and Suarez, 2001; Naaby-Hansen *et al.*, 2001) and the RyR (Trevino *et al.*, 1998; Harper *et al.*, 2004; Lefievre *et al.*, 2007) have been identified in mammalian spermatozoa. Although the exact functional role of RyRs located between the head and midpiece regions of the tail is less clear (for review see Costello *et al.*, 2009), the task of the IP_3-R is partially defined and depends on its compartmental expression pattern. On the one hand, the IP_3-R sited at the neck region of sperm (Ho and Suarez, 2003) has been suggested to play a role in sperm hyperactivation (for review see Olson *et al.*, 2011). On the other hand, the IP_3-R at the outer acrosomal membrane is operative in increasing Ca^{2+} in the periacrosomal cytoplasm, thereby triggering final steps of acrosomal exocytosis (De Blas *et al.*, 2002; Herrick *et al.*, 2005). Remarkably, local increase of Ca^{2+} originating from inside the acrosome is essential to trigger final fusion pore formation after capacitation-dependent docking of the vesicle and formation of a ready-to-go vesicle configuration (Maximov *et al.*, 2009; Tsai *et al.*, 2012). It is even central under conditions in which permeabilized spermatozoa are incubated in high external Ca^{2+} (De Blas *et al.*, 2002). Moreover, it was found that acrosomal Ca^{2+} alone is sufficient to trigger acrosomal exocytosis (Herrick *et al.*, 2005).

Of interest, in sea urchin sperm, sperm–egg binding led to an increase in cytosolic NAADP concentration (Churchill *et al.*, 2003). This observation, together with the acidic nature of NAADP-sensitive endolysosomal Ca^{2+} stores and the necessity of acrosomal Ca^{2+} to trigger zipper-like formation of hundreds of fusion pores (Harper *et al.*, 2008; Buffone *et al.*, 2009), raises the question of whether TPC channels facilitate the necessary Ca^{2+} signals. Therefore we investigated whether TPCs are expressed in mammalian spermatozoa and whether these channel proteins and/or their potential activator NAADP contribute to the acrosome reaction. To assess additionally whether such an NAADP pathway plays a functional role under physiological conditions, we quantified *Zona pellucida*–induced secretion rates in the presence of the NAADP antagonist *trans*-Ned-19.

RESULTS

Transcripts of two-pore channels in mouse testis

To evaluate initially whether two-pore channels are expressed in reproductive tissue, we performed reverse transcription (RT)-PCR analyses with TPCN1- and TPCN2-specific primer pairs and murine cDNA derived from testicular tissue and kidney expressing high levels of TPCs (Zong *et al.*, 2009). To validate cDNA synthesis, we first determined cDNA integrity derived from both tissues by using a primer pair against the housekeeping gene *β-actin* (Ziegler *et al.*, 1992). PCRs with the β-actin primer pair resulted in amplification fragments with the predicted size of 425 base pairs in kidney and testicular cDNA probes (Supplemental Figure S1, right, β-actin). Results of positive control RT-PCRs with kidney cDNA showed that PCR products with the expected size were successfully amplified for both TPC subtypes (TPCN1, 778 base pairs; TPCN2, 605 base pairs; Supplemental Figure S1, left, kidney). Examining cDNA derived from mouse testis, we found that amplicons with the calculated size for TPCN1 and TPCN2 were also detectable in testicular cDNA (Supplemental Figure S1, left, pair, testis). Subsequent subcloning and sequencing of the obtained PCR fragments confirmed the sequence identity with previously published murine TPCN1 (GenBank accession no. NM_145853.2) and TPCN2 (accession no. NM_146206.4) sequences.

Expression of TPC proteins in mammalian reproductive tissue

To determine whether the identified TPC1 and TPC2 transcripts are actually translated, we assessed testis and epididymis, as well as isolated spermatozoa, by means of Western blot analysis and immunohistochemical and immunocytochemical approaches, using subtype-specific antibodies. However, evaluating the specificity of commercially available anti-TPC1 and anti-TPC2 antibodies (Supplemental Materials and Methods) revealed no specific staining in

Western blotting or immunohistochemistry (unpublished data) when using kidney tissue as positive control (Ishibashi *et al.*, 2000; Zong *et al.*, 2009; Zhu *et al.*, 2010b). Therefore an anti-rabbit immunoglobulin G (IgG) antibody generated against a C-terminal peptide of the murine TPC1 (TPC1NK) was used (J.C. and N.K, unpublished data). Examination of the immunoreactivity of the TPC1NK antibody in Western blot analyses showed immunoreactive bands with the calculated size of TPC1 of ~94 kDa (*Mus musculus*, accession no. NP_665852; 94.36 kDa; Supplemental Figure S2, kidney TPC1 [+/+]) in mouse kidney tissue. These bands were detectable in the membrane protein fraction but not in the cytosolic fraction. The different sizes can be attributed to different glycosylation levels (Zong *et al.*, 2009). Moreover, expanding Western blot analyses to kidney tissue of homozygous TPC1-knockout mice, which served as negative controls (Ashton, 2011; Herkenham *et al.*, 2011), revealed no obvious TPC1-derived antibody labeling (Supplemental Figure S2, kidney TPC1 [–/–]), indicating high specificity of the TPCN1NK antibody.

Finally, we used the TPC1NK antibody to evaluate TPC1 protein expression in reproductive tissue, examining cytosolic and membrane samples of mouse testis and epididymis. Figure 1 shows that the TPC1NK IgG selectively labeled protein bands in testis (Figure 1A, TPC1 [+/+]) and epididymis (Figure 1B, TPC1 [+/+]) of wild-type animals, which were visible at the predicted molecular mass of murine TPC1. Comparing the intensity of the immunosignal in different subcellular fractions of both reproductive tissues, we found that staining was only detectable in membrane fractions (Figure 1, A and B, crude membrane pellet [P_2]) but not in cytosolic fractions (supernatant 2 [S_2]). This confirmed membrane localization of TPCs (Ishibashi *et al.*, 2000; Calcraft *et al.*, 2009; Zong *et al.*, 2009). Molecular identities of the immunoreactive bands were further confirmed by comparing immunostaining of testis and epididymis of TPC1-deficient mice, which did not show any immunoreactivity (Figure 1, A and B, TPC1 [–/–]).

Next we assessed whether TPC1 is also present in mature germ cells. We extended Western blot analyses to examine isolated epididymal rodent (rat, mouse) and ejaculated human spermatozoa. Initially, immunosignals were assessed on membrane fractions of mouse sperm by directly comparing staining patterns in membrane fractions of wild-type (Figure 1C, [+/+]) and TPC1-deficient spermatozoa (Figure 1C, [–/–]). Equal protein loading of tissue preparations of both mouse genotypes was verified using the raft marker protein caveolin-1 (Rothberg *et al.*, 1992; Parton, 1996). Figure 1C shows that wild-type spermatozoa show immunoreactive bands that center at the predicted molecular mass of the murine TPC1. Conspicuous smearing of the visible immunoreactive bands can be attributed to posttranslational glycosylation of two-pore channel proteins (Zong *et al.*, 2009). In contrast, assessing the labeling pattern in TPC1-deficient spermatozoa revealed no visible immunostaining. Comparing the labeling of rat spermatozoa, we found that the TPC1NK antibody stained a broad band with comparable molecular mass (Figure 1D) matching the size predicted from the rat-derived amino acid sequence (*Rattus norvegicus*, accession no. NP_647548; 94.28 kDa). The immunoreactive band was completely absent upon neutralizing the primary antibody with the immunogenic peptide (Figure 1D, Ab + BP), confirming TPC1-specific labeling. Moreover, the TPC1 immunoreactive signal selectively comigrated with the sperm-derived membrane fraction (Figure 1D), whereas the corresponding cytosolic protein fraction revealed no obvious immunostaining (unpublished data). Finally, to evaluate whether TPC1 is also expressed in human spermatozoa, we pooled ejaculated sperm of healthy donors and subjected it to membrane fractionation and separation via SDS–PAGE. Assessing immunostaining of the applied TPC1NK antibody, we found that the anti-TPC1NK IgG recognized bands with molecular masses ~100 kDa (Figure 1E), which corresponds well with the calculated molecular mass for human TPC1 (*Homo sapiens*, accession no. NP_001137291; 101.60 kDa). In addition, two smaller faint bands with a molecular mass of ~60 and 50 kDa, respectively, were visible.

To determine the subcellular expression pattern of TPC1, we used the TPC1NK antibody for classic indirect immunocytochemical staining, examining isolated epididymal mouse spermatozoa. Although numerous attempts were made to improve saturation of nonspecific binding sites of the anti-TPC1NK IgG (e.g., bovine serum albumin [BSA], fetal calf serum; unpublished data), TPC1-null sperm samples used as negative control did not allow conclusive exclusion of the possibility of partial nonspecific background labeling of the anti-TPC1NK antibody (unpublished data). Therefore TPC1 expression was evaluated on ultrathin sections of adult mouse testicular tissue of wild-type and TPC1-deficient males using immunogold electron microscopy. On examination of longitudinal sections of elongated mouse spermatides of TPC1-deficient animals (Figure 2, right, [–/–]), as well as sections of wild-type males, which were incubated with only gold-conjugated anti-rabbit IgG (unpublished data), no gold particles were detectable. However, in testis tissue of wild-type animals, prominent immunogold labeling was visible at the acrosomal sheath (Figure 2, TPC1 [+/+], arrowheads), whereas no gold particles were detected at the principal piece and midpiece region of the tail of wild-type sperm (Figure 2, TPC1 [+/+], arrows). Furthermore, it was apparent that colloidal gold labeling was restricted to a small region between the plasma membrane and the subacrosomal space (Figure 2, TPC1 [+/+], arrowheads). Remarkably, although inner and outer acrosomal membranes could not be distinguished due to the embedding procedure essential for electron microscopy (Weibull and Christiansson, 1986; Walensky and Snyder, 1995), the distribution of gold particles followed the contour of the outer acrosomal membrane, where they were arranged like pearls on a string.

NAADP-binding sites in epididymal mouse sperm visualized by the NAADP antagonist *trans*-Ned-19

Because the acrosome has been described as representing a specialized lysosome-related Ca^{2+} store (for review see Hartree, 1975; Costello *et al.*, 2009), we sought to assess whether NAADP-binding sites are present at the acrosomal region of spermatozoa. Living mouse sperm cells were incubated with the cell-permeable fluorescent NAADP antagonist *trans*-Ned-19 (Naylor *et al.*, 2009; Rosen *et al.*, 2009). Subsequently *trans*-Ned-19 emission was detected using a blue/cyan long-pass 4′,6-diamidino-2-phenylindole (DAPI) filter. To uncover possible autofluorescence of sperm at the excitation/emission wavelengths of *trans*-Ned-19 (355/415 nm), which may arise from endogenous fluorophores (Andersson *et al.*, 1998), we also took images from sperm incubated in capacitation buffer only. Figure 3A shows that the sperm head did not show any blue autofluorescence (Figure 3A, control, arrowhead), whereas the midpiece part of the flagellum emitted strong autofluorescence signals (Figure 3A, control, arrow). A comparison of the fluorescence emission of sperm loaded with *trans*-Ned-19 and capacitation buffer only confirmed a similar blue fluorescence emission signal at the midpiece of the sperm flagellum (Figure 3A, Ned19, arrow). However, two additional stained subcellular structures were detectable: we observed prominent labeling of the sperm neck (Figure 3B, Ned19, arrowhead), a membranous structure, which might represent an intracellular Ca^{2+}-storage site in mammalian spermatozoa (Ho and Suarez, 2001; Bedu-Addo *et al.*, 2008). In addition, an intense fluorescence signal was

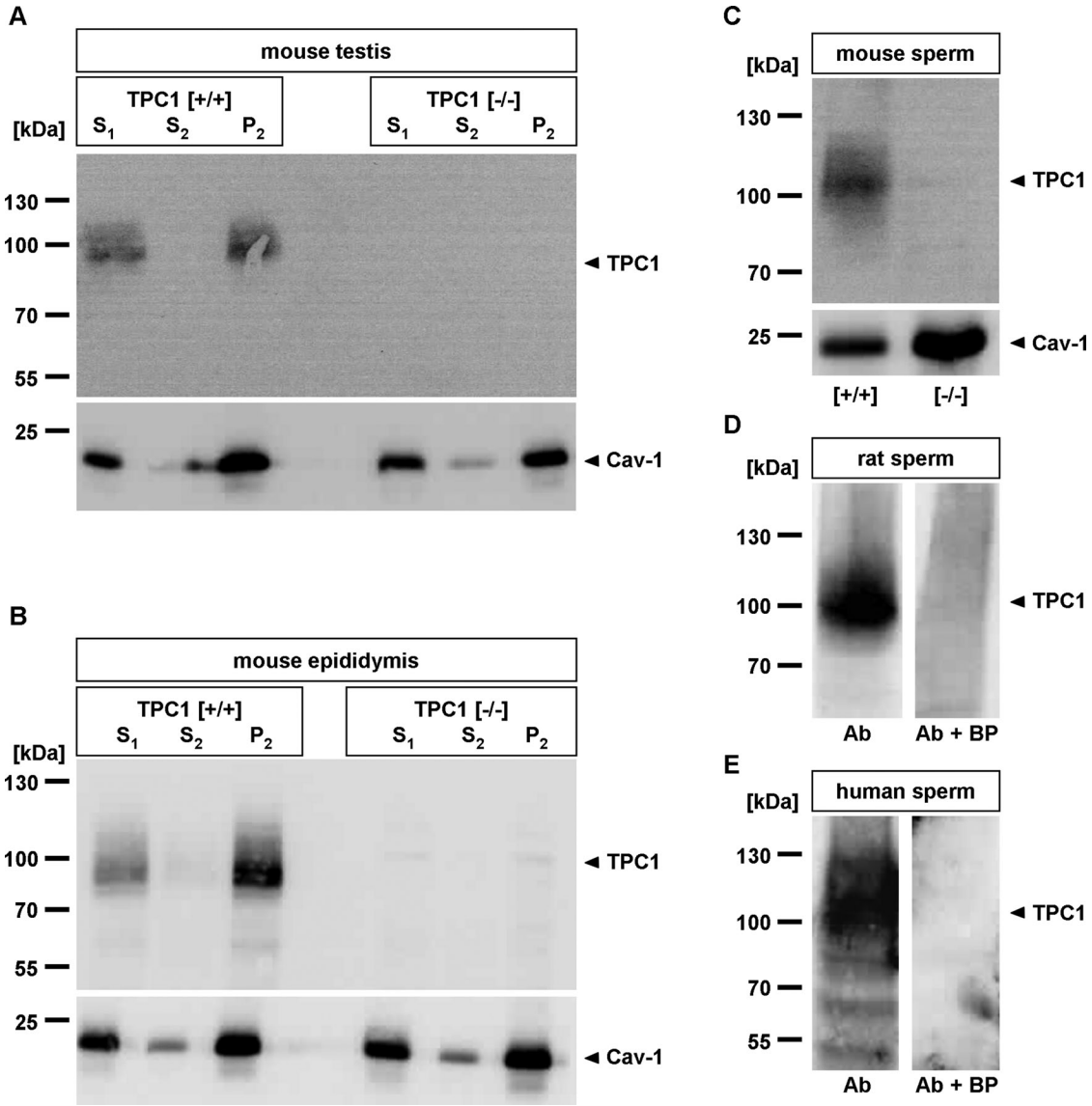

FIGURE 1: TPC1 expression in reproductive tissue and mammalian spermatozoa. (A, B) Expression and membrane localization of TPC1 in testicular and epididymal tissue. Equal amounts of crude tissue starting material (supernatant 1 [S_1]), as well as cytoplasmic (supernatant 2 [S_2]) and membrane extracts (P_2) of mouse wild-type (TPC1 [+/+]) and TPC1-deficient (TPC1 [–/–]) testis (A) and epididymis (B), were subjected to SDS–PAGE and assayed for TPC1 immunoreactivity using the anti-TPC1NK antibody. Equal protein loading of tissue fractions derived from both genotypes was verified using an antibody recognizing the raft marker protein caveolin-1 (Cav-1). Note that in wild-type samples the anti-TPC1NK IgG-labeled immunoreactive bands were centered at a molecular mass of ~94 kDa in testis (A) and epididymis (B), whereas in reproductive tissue of TPC1-null animals no immunostaining was detectable. Comparing the labeling in the cytosolic (S_2) and membrane fractions (P_2), it is evident that the immunoreactive bands were always enriched in the corresponding membrane protein fractions, whereas the cytosolic extracts showed no obvious immunoreactivity. (C–E) Identification of TPC1 in rodent and human spermatozoa by immunoblot analysis. Equal amounts of membrane fractions of mouse spermatozoa of TPC1 wild-type ([+/+]) and TPC1-knockout mice ([–/–]; C) and membrane fractions of rat spermatozoa (D), as well as human sperm membranes (E), were separated by SDS–PAGE and probed with the anti-TPC1NK IgG. On monitoring of sperm preparations of the three species for immunoreactivity, bands with the expected size for TPC1 of ~94 kDa for rodents and ~100 kDa for humans were visible. The immunoreactive bands with higher molecular masses indicate glycosylated forms of TPC1. Specificity of immunostaining in rat and human sperm was confirmed upon neutralization of the primary antibody with the immunogenic peptide (D and E, Ab + BP). For mouse sperm, germ cells of TPC1-knockout animals were examined as negative control (C, [–/–]). A, B, and D show representatives of at least three independent experiments with tissue preparations of different animals. For separated mouse (C, 19 animals) and human sperm (E, ejaculates of three healthy volunteers), germ cells were pooled and fractionated; membrane proteins were subjected at least three times to Western blot analyses. The caveolin-1 blot (Cav-1) served as loading control for epididymal mouse sperm. Left, positions of the molecular weight standards in kilodaltons for each Western blot.

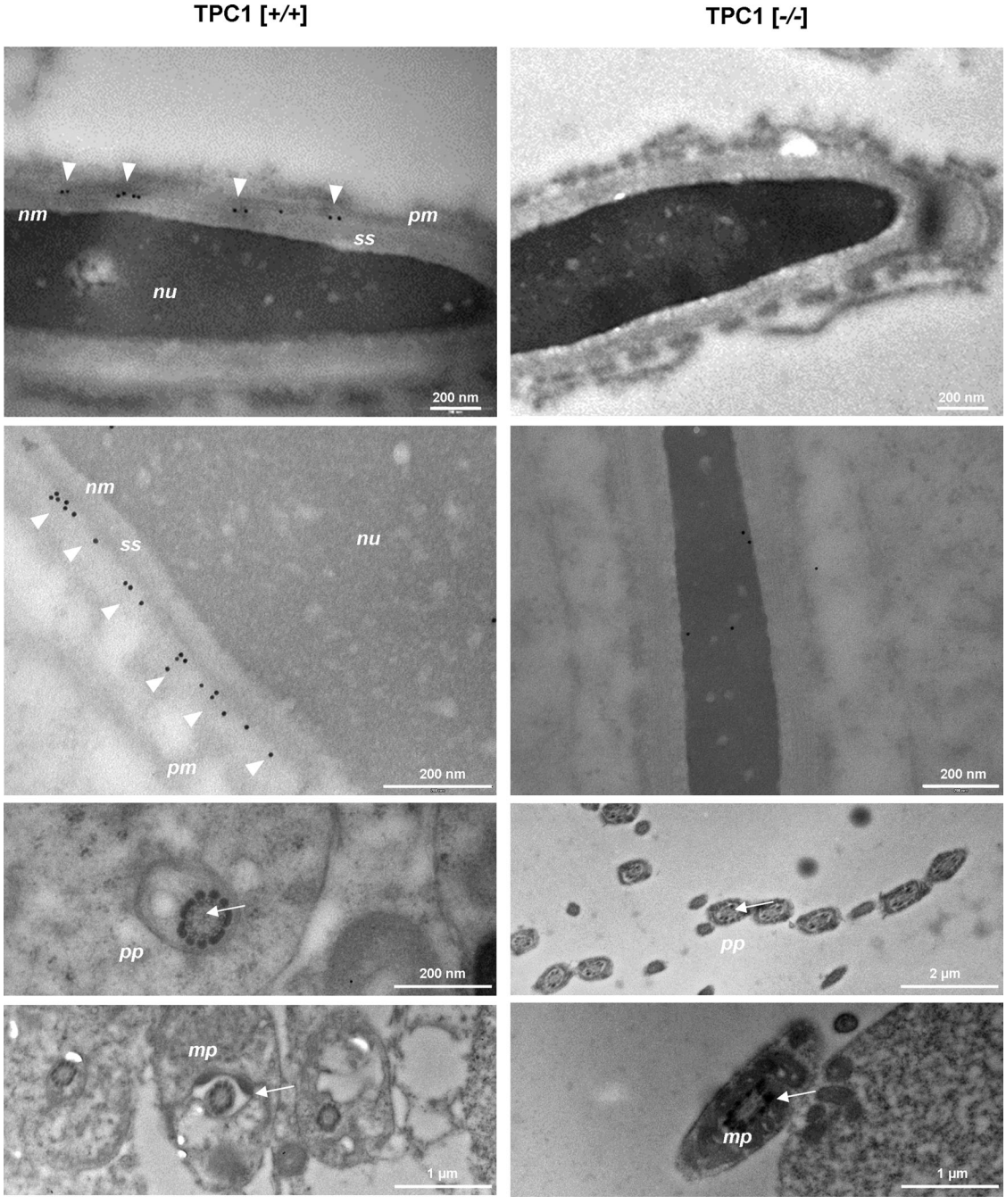

FIGURE 2: Immunoelectron microscopic analysis of TPC1 in adult mouse testis. Ultrathin sections of adult mouse testis of wild-type (left, TPC1 [+/+]) and TPC1-knockout males (right, TPC1, [–/–]) were labeled with anti-TPC1NK antibody, followed by incubation with goat anti-rabbit IgG conjugated to colloidal gold particles. TPC1-null testis tissue and the midpiece (mp) and proximal part of the principal piece (pp) of sperm tails of wild-type males did not show any precipitated immunogold particles. However, in wild-type spermatides, immunogold particles were only detected at a narrow area between the plasma membrane (pm) and the subacrosomal space (ss). This area holds membranes lining the acrosome. Although these membranes were only poorly preserved due to the fixation and embedding procedure, gold particles were found to follow the contour of the outer acrosome membrane. Images in the second line show different tissue areas with similar gold particle distribution. nm, nuclear membrane; nu, nucleus.

visible at the convex side of the sperm head (Figure 3, A, Ned19, arrowhead, and B, Ned19, arrowhead), indicating NAADP-binding sites at two distinct intracellular Ca^{2+} reservoirs. To determine whether NAADP-binding sites at the sperm head are indeed localized to the acrosomal region, we used an acidotropic membrane-permeable fluorescent probe, LysoTracker Red, which typically concentrates within the acrosome due to its luminal acidic pH (Moreno *et al.*, 2000; Sun-Wada *et al.*, 2002). Figure 3B shows that capacitated epididymal sperm incubated with LysoTracker Red displayed an intense labeling of the acrosome (Figure 3B, Lyso, arrowhead), which showed the same subcellular location as *trans*-Ned-19 (Figure 3B, Ned19, arrowhead). The observation that NAADP-binding sites were indeed

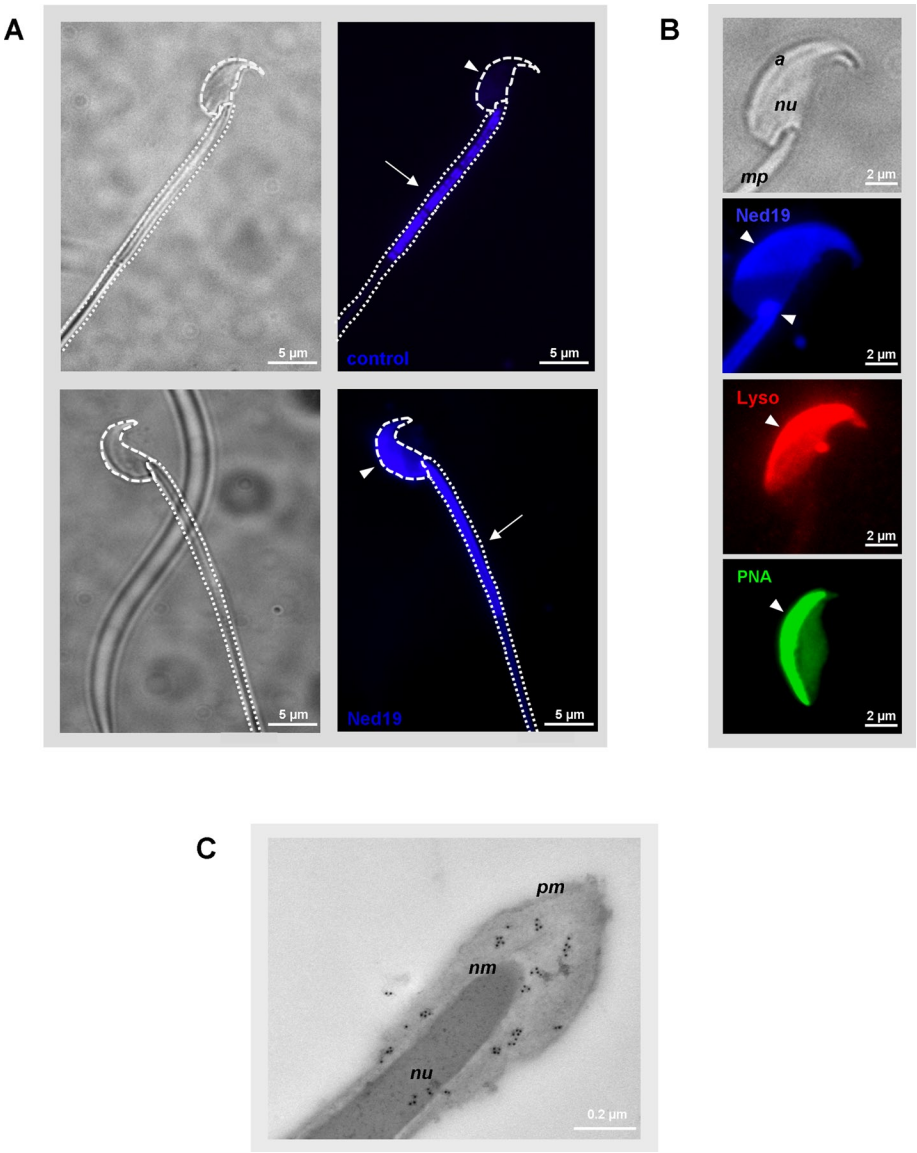

FIGURE 3: Localization of NAADP-binding sites and TPC1 in mouse spermatozoa. (A) Subcellular localization of *trans*-Ned-19–binding sites in murine sperm. Epididymal mouse sperm were incubated with 100 µM fluorescent NAADP antagonist *trans*-Ned-19 (Ned19), and subsequently binding of *trans*-Ned-19 was examined microscopically. To visualize autofluorescence under the excitation/emission conditions of *trans*-Ned-19, control sperm were incubated in the corresponding buffer only. Note that *trans*-Ned-19–loaded sperm not only show autofluorescence-derived tail staining, as observed for untreated sperm (control, arrow), but in addition are characterized by an intense blue fluorescence signal located at the neck region (Ned19, arrowhead], as well as at the acrosomal cap (Ned19, arrowhead). The dotted lines in the phase-contrast picture (right, top micrograph) border the sperm's head and the flagellum. Micrographs show representative images of at least three different sperm preparations with comparable results. (B) *Trans*-Ned-19 binding is localized to the acrosomal region. Isolated epididymal mouse sperm were probed with *trans*-Ned-19 (Ned19, blue), the fluorescent acidotropic dye LysoTracker Red (Lyso, red), or the FITC-conjugated acrosomal marker PNA (green), illustrating the position of the hook-shaped acrosome. Note that staining with PNA as well as with LysoTracker Red shows the same subcellular distribution as labeling with *trans*-Ned-19. The light micrograph of the mouse sperm head (top) marks the sperm nucleus (nu), the apical acrosomal region (a), and part of the midpiece of the sperm tail (mp). Arrowheads mark positive sperm acrosomal labeling. (C) Distribution of TPC1 in epididymal mouse spermatozoa visualized via immunogold electron microscopy. Ultrathin sections of adult mouse epididymis were labeled sequentially with anti-TPC1NK antibody, followed by incubation with gold-conjugated anti-rabbit IgG. Note that immunogold particles are predominantly localized at the acrosomal region of the sperm head between residues of the plasma membrane (pm) and the nuclear membrane (nm). A few colloidal particles were also found associated with the condensed DNA in the nucleus (nu).

restricted to the acrosomal cap was further confirmed using the acrosomal lectin marker peanut agglutinin (PNA; Aviles *et al.*, 1997; Figure 3B, PNA, arrowhead). Examining the ultrastructural localization of TPC1 in epididymal spermatozoa, we again performed indirect immunogold electron microscopy. Of interest, we found that colloidal gold particles were predominantly localized at the acrosomal tip. However, immunostaining was also detectable at the postacrosomal region, where it was mainly concentrated between the plasma membrane and the nuclear membrane (Figure 3C), indicating colocalization with apparent NAADP-binding sites (Figure 3B, Ned19).

Reproductive success of TPC1-deficient mice

Our results indicate that TPC1 is present in membrane fractions of testis and epididymis, as well as in mature spermatozoa of different mammalian species (Figure 1). Specifically, TPC1 immunoreactivity is localized to the acrosomal region (Figures 2 and 3C). Next we evaluated whether TPC1 plays a functional role for successful fertilization. We set up a systematic breeding scheme with 8– to 16-wk-old homozygous ([–/–]), heterozygous ([+/–]), and wild-type ([+/+]) TPC1 mice. We analyzed litters for TPC1-dependent alterations. We found that mice bearing a null mutant in the *TPCN1* gene were viable and grew normally with no apparent malformation. Moreover, quantifying standard reproduction parameters revealed that all heterozygous and homozygous TPC1-null breeding pairs were successful in producing litters and showed no obvious impairment in fertility regarding mean number of offspring per litter or sex distribution among offspring (Table 1). However, examination of time intervals needed to successfully deliver showed that lack of TPC1 protein resulted in a longer time needed to produce pups (Table 1), although the results are not statistically significant: whereas wild-type crosses ([+/+] × [+/+]) needed 33.6 ± 2.3 d between consecutive litters, homozygous TPC1 breeding pairs required 4 d longer (Table 1, [–/–] × [–/–], 37.1 ± 2.5 d); heterozygous mating pairs needed intermediate intervals to successfully produce offspring (Table 1; [+/–] × [+/–], 34.5 ± 1.3 d).

A reproductive phenotype of a knockout line can often only be recognized by comparing the genotype distribution of pups obtained from heterozygous mating pairs with the predicted Mendelian ratio of offspring ([+/+]:[+/–]:[–/–] = 1:2:1; Montoliu, 2012). Thus we calculated the frequency of genotypes of offspring from heterozygous TPC1 mating pairs. Of 681 genotyped pups

Reproduction parameter	Genotype of mating partners		
	[+/+] × [+/+]	[+/–] × [+/–]	[–/–] × [–/–]
Litter size (breeding pairs/ litter)	6.4 ± 0.2 (8/30)	6.5 ± 0.1 (26/105)	6.2. ± 0.2 (8/31)
Gender (% males)	57.1	52.8	48.5
Time to litter (d)	33.6 ± 2.3	34.5 ± 1.3	37.1 ± 2.5

In a continuous breeding study, fertility of TPC1-deficient breeding pairs (heterozygous [+/–] × [+/–], homozygous [–/–] × [–/–]), and wild-type animals ([+/+] × [+/+]) was estimated by determining number of pups per litter (litter size), sex ratio of pups (% males), and days between subsequent litters (time to litter). Numbers in parentheses indicate number of mating pairs and number of litters, respectively.
Data represent mean values ± SEM; statistical analyses of litter size and time to litter were performed using an unpaired Student's *t* test comparing data of TPC1-deficient mating and wild-type breeding pairs. Chi-squared test was used to determine whether the sex ratio differed from the theoretical inheritance mode (1:1); $p < 0.05$ was considered to be statistically significant.

TABLE 1: Fertility and outcome of systematic breeding of TPC1-deficient mice.

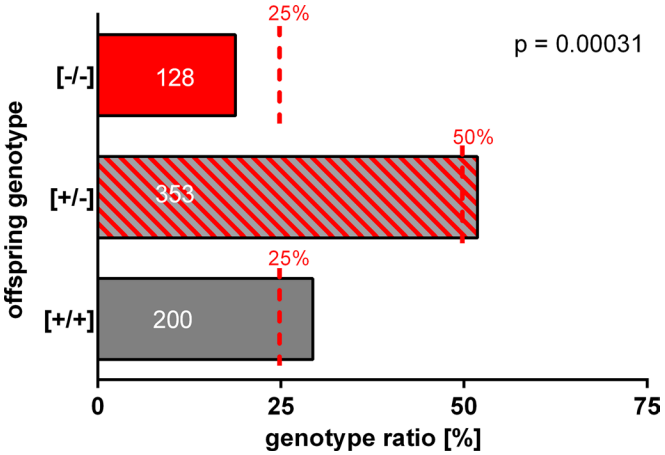

FIGURE 4: Genotype distribution of pups produced by heterozygous TPC1 breeding pairs. Frequency of genotypes of offspring from heterozygous TPC1 mating pairs was determined in a continuous breeding study. Columns represent the percentage of the registered genotype of offspring; dashed red lines indicate expected frequency based on Mendelian inheritance. Note that heterozygous intercrosses produced fewer TPC1-mutant mice ([–/–]) than predicted from the Mendelian distribution. Only 128 of 681 weaned pups from 105 litters were homozygous for TPC1, resulting in a significant deviation from Mendelian distribution of TPC1-null pups. Data present the ratio of offspring of 26 heterozygous TPC1 breeding pairs. Numbers in the columns represent numbers of pups for each genotype. The significance of deviation from expected Mendelian ratio was tested using chi-squared statistics.

from 105 litters, 51.84% were heterozygous for TPC1. However, the percentage of pups with wild-type genotype was elevated (Figure 4; 29.37%) and the proportion of TPC1-null animals born was reduced (18.80%; deviation from Mendelian ratio, $p = 0.00031$). Because 25% of pups derived from heterozygous breeding pairs should be homozygous for TPC1, one might suggest that TPC1 deletion results in an overt subfertile reproductive phenotype (Langa *et al.*, 2003).

To understand the reason for the divergence from the Mendelian inheritance ratio, we examined the effect of TPC1 deletion on testis morphology and germ cell number of sexually mature wild-type, heterozygous, and homozygous TPC1 animals. Data summarized in Table 2 show that TPC1-null males had a slightly but not significantly ($p = 0.188$) reduced weight compared with wild-type mice; similarly, testis to body weight ratio of TPC1-null animals (0.77 ± 0.01%) was reduced compared with wild-type animals (0.79 ± 0.01%). To analyze whether the reduced testis weight has any effect on the dimension and/or cellular organization of seminiferous tubules, we examined histological hematoxylin-eosin–stained sections of testes of TPC1 knockout animals and compared them with wild type. As observed for the ultrathin sections examined with electron microscopy (Figure 2), no obvious morphological abnormalities were visible on comparing testes of TPC1-null males with wild-type animals. The number and diameter of seminiferous tubules within the testis were not reduced (unpublished data). The tubules exhibited the full spectrum of ordered concentric layers of developing germ cells, such as spermatogonia, spermatocytes, and spermatids (Supplemental Figure S3A, left pair; Chu and Shakes, 2012). The same was true for the epididymis—the storage organ for mature spermatozoa (Robaire *et al.*, 2002)—whose epididymal ducts in the caudal and caput regions were equally filled with mature spermatozoa (Supplemental Figure S3A, right pair, arrow).

Because these observations suggest no considerable defects in spermatogenesis upon *TPCN1* gene deletion, we sought to examine the morphology and physiological function of mature caudal spermatozoa of TPC1-deficient males. No obvious morphological defects of TPC1-null sperm were detectable in light microscopic examinations of Coomassie blue–stained epididymal spermatozoa. TPC1-deficient germ cells possessed a regularly formed straight tail and a falciform head with the typical apical hook (Supplemental Figure S3B, CB). Moreover, in selective staining experiments with fluorescence-conjugated PNA, the typical crescent moon shape of the acrosome was visible (Supplemental Figure S3B, PNA). Next we assessed whether TPC1 deletion has any effect on NAADP binding. We incubated epididymal spermatozoa of wild-type and TPC1-null sperm of littermate males with the NAADP antagonist *trans*-Ned-19 and examined them by fluorescence microscopy. Although quantification of *trans*-Ned-19 labeling was not possible because *trans*-Ned-19 shows disturbing fluorescence recovery after photobleaching (Meyvis *et al.*, 1999),

Reproduction parameter	Genotype		
	[+/+]	[+/–]	[–/–]
Testis to body weight ratio (%)	0.79 ± 0.01 ($n = 40$)	0.77 ± 0.01 ($n = 28$)	0.77 ± 0.01 ($n = 31$)
Testis weight (mg)	104.7 ± 1.2 ($n = 91$)	102.1 ± 1.5 ($n = 52$)	101.7 ± 2.1 ($n = 57$)
Sperm count ($\times 10^6$)	28.5 ± 1.0 ($n = 45$)	27.6 ± 1.3 ($n = 38$)	23.7 ± 1.1** ($n = 30$)

Adult male homozygous ([–/–]), heterozygous ([+/–]), and wild-type animals ([+/+]) with identical strain background and age were analyzed for total body weight, testis weight (one testis), and number of sperm in the caudal part of the epididymis. Note that the total number of sperm was significantly different ($p = 0.0031$) in homozygous TPC1-deficient males compared with wild-type animals. Data are mean values ± SEM of 30–91 animals. Statistical analysis was done using an unpaired Student's *t* test comparing parameters of the two TPC1-deficient genotypes with wild-type animals (**$p < 0.01$).

TABLE 2: Effect of TPC1 deficiency on testis weight and number of caudal epididymal sperm.

trans-Ned-19–derived acrosomal staining of TPC1-null sperm was found to show the same acrosomal localization and comparable signal intensity as fluorescence labeling of sperm of TPC1 [+/+] littermates (Supplemental Figure S3B, Ned19). However, quantifying total sperm counts isolated from the epididymis led to an interesting observation (Table 2). In homozygous TPC1 [–/–] mice the number of sperm cells was reduced ([23.8 ± 1.2] × 10^6; p =0.0031) compared with age-matched wild-type animals ([28.6 ± 1.0] × 10^6). Total sperm counts from heterozygous TPC1 mice showed values that were intermediate between those derived from wild-type and TPC1-null animals ([27.6 ± 1.3] × 10^6).

NAADP can trigger acrosome reaction in the absence of extracellular Ca^{2+}

The observation that efflux of Ca^{2+} from the acrosomal storage site is necessary to trigger the final exocytotic fusion step downstream of the vesicle-associated small GTPase Ras-like guanine nucleotide–binding protein (Rab3A; De Blas *et al.*, 2002) and the visualization of NAADP-binding sites at the acrosomal region (Figure 3B) prompted us to test whether NAADP is able to trigger acrosome reaction in mouse sperm. However, using the cell-permeant prodrug of NAADP (acetoxymethyl ester of NAADP [NAADP-AM]) does not allow assessment of the exact concentration of active NAADP within a cell. Therefore we permeabilized the sperm plasma membrane with the bacterial toxin streptolysine O (SLO; Johnson *et al.*, 1999; Hutt *et al.*, 2005; Ackermann *et al.*, 2009). Thus we were able to introduce negatively charged NAADP into the cytosol of spermatozoa. However, this approach also allowed us to restrain acrosomal secretion to the final fusion step of pore formation: Given that the permeabilization of sperm required a transfer into Ca^{2+}-free external solution (Tomes, 2007; *Materials and Methods*), local increase in Ca^{2+}, essential for final fusion pore formation, solely originated from the acrosomal storage site (Rossato *et al.*, 2001; De Blas *et al.*, 2002; Herrick *et al.*, 2005; Tsai *et al.*, 2010; Bello *et al.*, 2012).

To investigate the effect of NAADP on acrosomal secretion, we incubated capacitated and SLO-permeabilized epididymal mouse sperm in Ca^{2+}-free KRB buffer supplemented with different NAADP doses. We then quantified the acrosomal status. The specificity of NAADP effects was assessed in parallel approaches in which cells were incubated with equal concentrations of the inactive linear precursor of NAADP, nicotinamide adenine dinucleotide phosphate (NADP; Lee, 2001; Galione *et al.*, 2009). Furthermore, since physiological acrosome reaction can only occur in fully capacitated spermatozoa (Sutton *et al.*, 2008; Abou-Haila and Tulsiani, 2009), we determined the ability of NAADP to increase the incidence of acrosome reaction in uncapacitated sperm. These control experiments with uncapacitated germ cells never showed a significant increase in acrosomal secretion rates (Supplemental Table S1).

Mobilization of Ca^{2+} from acidic intracellular stores is already elicited at low, submillimolar NAADP concentrations (for review see Galione and Ruas, 2005). Therefore we initially determined a dose–response relationship for NAADP by incubating sperm for a NAADP concentration range of 10–100 nM. Figure 5A shows that NADP over the whole concentration range increases acrosomal secretion rates only to ~1–2% above the spontaneous loss of the acrosomal vesicle. However, NAADP elicited a much stronger and dose-dependent increase in exocytosis with an apparent saturation at ~50 nM. Of interest, adding slightly higher NAADP doses (75, 100 nM) led to a steady decline in acrosome-reacted sperm, resulting in the characteristic self-inactivation phenomenon of NAADP-elicited responses (Cancela *et al.*, 1999; Berg *et al.*, 2000; Galione and Ruas, 2005; Galione, 2011; Tugba Durlu-Kandilci *et al.*, 2010; Zhang *et al.*, 2012). So far the data suggest that NAADP is able to trigger acrosome reaction in permeabilized sperm and that additional extracellular Ca^{2+} is not required. Next we assessed whether other NAADP targets with lower NAADP affinities were also involved in triggering acrosomal exocytosis. We used a higher concentration range of NAADP and NADP (250 nM to 100 µM). Figure 5B shows that sperm incubated with higher NAADP doses underwent significant acrosomal exocytosis with one additional bell-shaped curve, which peaked at 1 µM NAADP, whereas NADP elicited significant acrosomal secretion only at extremely high doses (100 µM). Of interest, data on the full dose relationship for NAADP (Figure 5, A and B) showed that the two clearly detectable maxima of NAADP-evoked responses at submillimolar NAADP doses (50 nM, 1 µM) are in striking agreement with intracellular NAADP concentrations determined for ligand-induced NAADP accumulation (Churchill *et al.*, 2003; Masgrau *et al.*, 2003; Yamasaki *et al.*, 2005; Gasser *et al.*, 2006; Lewis *et al.*, 2012; Schmid *et al.*, 2012). Thus NAADP elicited acrosomal exocytosis could already be detected at physiological purine nucleotide concentrations.

A specific feature of NAADP-induced cellular reactions is a selective inhibition by its noncompetitive antagonist *trans*-Ned-19 (Churchill and Galione, 2000; Naylor *et al.*, 2009; Rosen *et al.*, 2009; Pitt *et al.*, 2010). Therefore we next investigated the effect of *trans*-Ned-19 on NAADP-evoked acrosome reaction. First we assessed whether *trans*-Ned-19 has any effect on spontaneous loss of the acrosome of capacitated mouse sperm. However, half-maximal inhibitory concentration of *trans*-Ned-19 strongly depends on the examined cell type (Naylor *et al.*, 2009; Rosen *et al.*, 2009; Arredouani *et al.*, 2010; Ruas *et al.*, 2010). Therefore effects of *trans*-Ned-19 on the incidence of spontaneous acrosome reaction were first determined for low (100 nM) and high (100 µM) *trans*-Ned-19 concentration. The results summarized in Figure 5C show that treatment of permeabilized sperm with 100 nM *trans*-Ned-19 (Figure 5C, +0.1 µM Ned19) did not significantly affect acrosomal status compared with sperm incubated with control buffer (Figure 5C, control). However, upon application of 100 µM *trans*-Ned-19, spontaneous acrosome reaction rate was significantly increased (Figure 5C, +100 µM Ned19, p = 0.0020). Remarkably, 100 µM *trans*-Ned-19 was also found to slightly potentiate NAADP-induced acrosomal secretion rates (Supplemental Figure S4A). Moreover, increase in cytosolic Ca^{2+} was elicited upon treating capacitated sperm with 100 µM *trans*-Ned-19 (Supplemental Figure S4B). Thus high *trans*-Ned-19 concentrations seem to mimic the action of NAADP (Pitt *et al.*, 2010). Consequently, we evaluated whether a *trans*-Ned-19 dose that did not affect spontaneous acrosomal secretion antagonizes NAADP-induced acrosome reaction. Permeabilized sperm were either transferred to KRB buffer supplemented with NAADP, or acrosomal exocytosis elicited by NAADP was initiated in the presence of 100 nM *trans*-Ned-19. Because the results of our dose–response analyses reveal maximal responses at two NAADP doses, the effect of 100 nM *trans*-Ned-19 was determined for 50 nM and 1 µM NAADP peak concentrations (Figure 5, A and B). In addition, 50 µM was applied as a control throughout to ensure NAADP delivery to the cell (Figure 5, A and B). Moreover, acrosomal secretion rates were calculated as percentages of maximal responses registered upon treatment of sperm with high extracellular Ca^{2+} (*Materials and Methods*, acrosomal exocytosis index) to make results comparable to other presented experiments. Data illustrated in Figure 5D show that low *trans*-Ned-19 doses attenuated responsiveness induced by all three NAADP doses. However, significant inhibitory effects were only detectable at low NAADP doses: at 50 nM NAADP, the acrosomal secretion rate was attenuated to 14.2 ± 3.2%

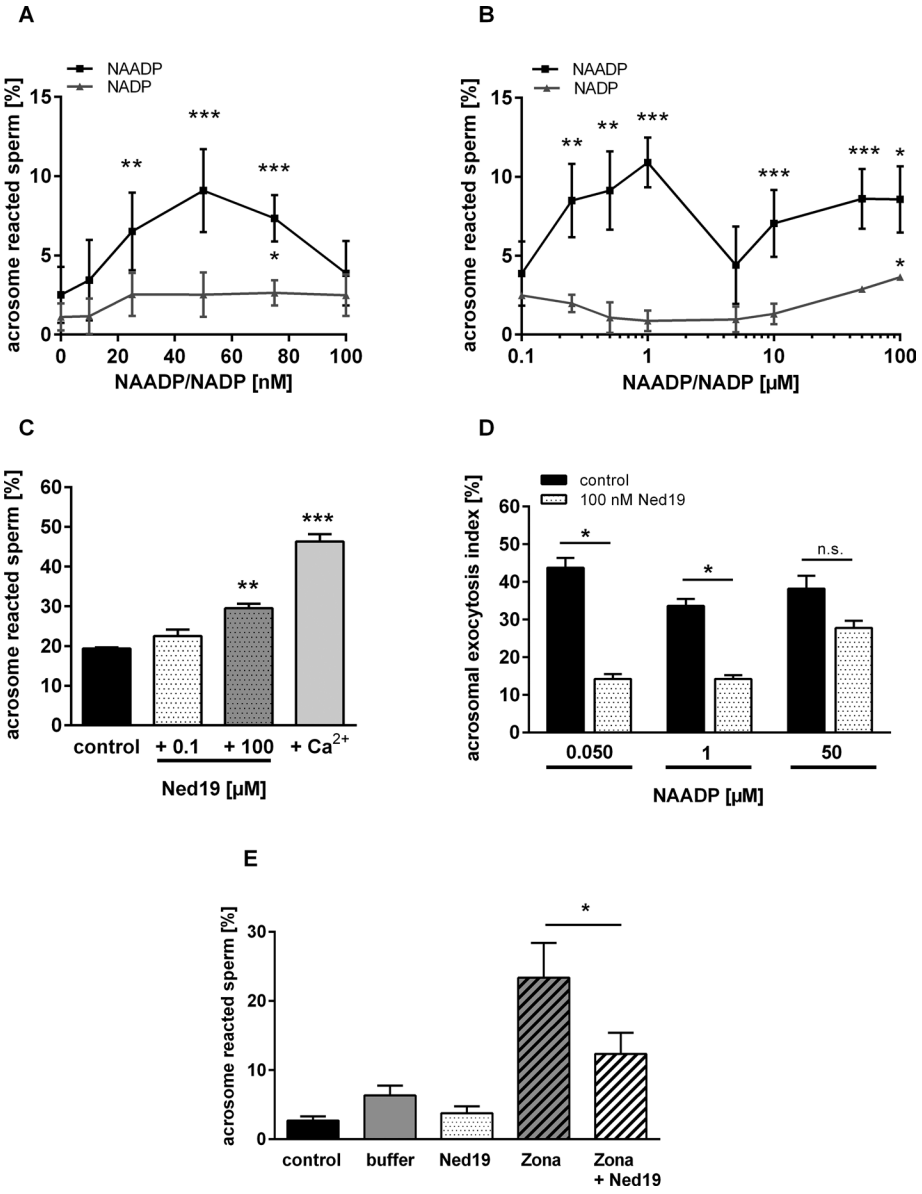

FIGURE 5: Effects of NAADP and its antagonist *trans*-Ned-19 on acrosome reaction. (A) Concentration response curve of low doses of NAADP on acrosome reaction in spermatozoa isolated from BALB/c mice. To evaluate whether NAADP or its structurally related metabolic precursor NADP influences acrosome reaction, capacitated epididymal spermatozoa were permeabilized with the bacterial toxin SLO and treated for 30 min at 37°C with a narrow range of low doses of either NAADP or NADP (10–100 nM), respectively. Subsequently, acrosomal status was blindly quantified by counting a minimum of 200 sperm/slide. The percentage of induced acrosome reaction of NAADP-reacted sperm over the whole applied concentration spectrum was calculated. A significant elevation in acrosomal exocytosis was visible, following a bell shape with a maximal response at ~50 nM NAADP. In contrast, NADP-treated sperm showed only weak increase in the percentage of acrosome-reacted sperm. (B) Elevation of acrosome reaction monitored over a high concentration range of NAADP and NADP. To assess the effect of high NAADP doses, a concentration range of 100 nM to 100 µM was applied. Note that the inactive analogue NADP only elicited significant acrosomal secretion at extremely high (100 µM) concentrations. However, NAADP induced significant acrosomal secretion with maxima at 1 and 50 µM NAADP, respectively. Data in A and B are mean values ± SEM and were normalized by subtracting the percentage of acrosome-reacted spermatozoa of each experiments after 90-min capacitation (NAADP: 14.6 ± 1.7%; NADP: 9.1 ± 1.3%). The data were collected from independent experiments (5 NADP; 14 NAADP) with different mouse sperm preparations. Statistical significance (*$p < 0.05$, **$p < 0.01$, ***$p < 0.001$) was considered if data were different from rates of spontaneous loss of the acrosomal vesicle (A, 0 nM NAADP/NADP). (C) Effect of the NAADP antagonist *trans*-Ned-19 on spontaneous acrosome reaction. Capacitated and permeabilized mouse spermatozoa were incubated for 30 min in KRB/SLO buffer or in permeabilization buffer supplemented with either low (100 nM) or high (100 µM) *trans*-Ned-19 doses. Efficiency of SLO permeabilization was verified by stimulating sperm with 10 mM $CaCl_2$ (Ca^{2+}). Note that in the presence of high *trans*-Ned-19 concentration, spontaneous loss of the acrosomal vesicle was significantly elevated compared with samples incubated in control buffer. Low *trans*-Ned-19 did not affect basal acrosomal status. Data represent the mean values of acrosome reacted sperm ± SEM of six independent experiments with different mouse sperm preparations (***$p < 0.001$) compared with samples incubated in KRB/SLO buffer only (control). (D) Effect of 100 nM *trans*-Ned-19 on NAADP-induced acrosome reaction. To assess whether low *trans*-Ned-19 concentrations antagonize NAADP-induced acrosome reaction, capacitated and permeabilized sperm were stimulated with either NAADP doses found to elicit maximal acrosomal secretion rates (50 nM, 1 µM, 50 µM) or one of the three NAADP doses together with *trans*-Ned-19. Note that 100 nM *trans*-Ned-19 significantly reduced responsiveness induced by 50 nM and 1 µM NAADP, whereas acrosomal secretion elicited by 50 µM NAADP was only slightly attenuated. Results presented are mean values ± SEM of acrosomal exocytosis index and are the average of six independent experiments. Statistical significance (paired Student's *t* test; $p < 0.05$; n.s., not significant) was calculated by comparing samples only stimulated with one of the three NAADP doses with corresponding probes incubated with NAADP together with *trans*-Ned-19. (E) Effect of *trans*-Ned-19 on *Zona pellucida*–induced acrosome reaction. To assess whether an NAADP-controlled signaling pathway is operative in driving acrosomal exocytosis under physiological conditions, capacitated but nonpermeabilized sperm were treated for 30 min at 37°C with solubilized *Zona pellucida* (10 zonae/µl cell suspension), or, alternatively, *Zona pellucida* stimulation was performed in the presence of the NAADP antagonist *trans* Ned-19 (100 nM). Note that *Zona pellucida* stimulation elevated exocytosis to a mean value of ~23.35 ± 5.04% (Zona) compared with sperm incubated in the respective buffer used to solubilize and dilute isolated *Zona pellucida* (buffer: 6.31 ± 1.43%). However, simultaneous application of *trans*-Ned-19 resulted in a significant ($p < 0.013$) reduction in acrosomal exocytosis (Zona + Ned19: 12.33 ± 3.06%). Data, calculated as absolute percentages of acrosome-reacted sperm, represent mean values ± SEM of five independent experiments with different mouse sperm preparations. Statistical significance (*$p < 0.05$) was considered if data were different from secretion rates of germ cell samples stimulated with purified *Zona pellucida*.

compared with the signal induced by NAADP alone ($p = 0.015$), whereas at 1 µM NAADP a significant reduction to 14.2 ± 2.5% was seen ($p = 0.011$).

The physiological ligand to drive the acrosome reaction is the *Zona pellucida* of the mature oocyte (Wassarman, 2008). To assess whether NAADP is indeed functionally involved in physiological acrosome reaction, we quantified the effect of *trans*-Ned-19 on *Zona pellucida*–induced acrosome reaction. Capacitated and nonpermeabilized sperm were simultaneously treated with solubilized *Zona pellucida* and 100 nM *trans*-Ned19 before the acrosomal status was quantified. Figure 5E shows that stimulation of spermatozoa with *Zona pellucida* elevated the exocytosis to a mean of ~23.35 ± 5.04% (Figure 5E; *Zona*), whereas secretion rates of sperm incubated in buffer used to dilute *Zona* only slightly increased (buffer: 6.31 ± 1.43%) compared with spontaneous loss of the acrosomal vesicle (control: 2.68 ± 0.61%). Comparison of the effect of germ cells incubated with *trans*-Ned-19 together with solubilized *Zona pellucida* showed significant ($p = 0.0136$) reduction in acrosomal exocytosis (*Zona* + *Ned19*: 12.33 ± 3.06%).

These results indicate that an NAADP-pathway indeed triggers acrosome reaction in spermatozoa under physiological conditions. However, since the IP_3-R was found to be also functionally operative in inducing acrosome reaction by mobilizing Ca^{2+} from the acrosomal storage site (Herrick *et al.*, 2005; Zanetti and Mayorga, 2009), we next examined a possible functional interrelation between the acidic acrosomal Ca^{2+} storage site and the ability of NAADP to trigger acrosome reaction. Although the functional role of the RyR in mammalian sperm is less clear (for review see Costello *et al.*, 2009), we also tested its involvement in the NAADP-triggered acrosome reaction. We used selective antagonists of the two most common intracellular Ca^{2+} channels, ruthenium red (RR) for the RyR (Tapia and Velasco, 1997) and 2-aminoethyldiphenyl borate (2-APB) for the IP_3-R (Maruyama *et al.*, 1997). In initial control experiments in which capacitated and permeabilized mouse sperm were incubated in buffer supplemented with either 2-APB or RR, no effects of the two inhibitors were detectable on spontaneous acrosomal exocytosis (Supplemental Figure S5A). Next we examined the effects of RR and 2-APB at distinct NAADP doses triggering maximal secretion responses (Figure 5, A and B, 50 nM, 1 µM, 50 µM). Supplemental Figure S5B shows that RR slightly attenuates acrosome reaction rates at all three NAADP concentrations. However significant effects were detectable only at very high NAADP doses (Supplemental Figure S5B, 50 µM NAADP). With regard to the effect of the IP_3-R antagonist 2-APB, a more pronounced and significant attenuation was registered for all three applied NAADP doses, with the strongest inhibition detectable at the two low physiological NAADP doses (Supplemental Figure S5C, 50 nM and 1 µM NAADP).

Our observation of a colocalization of NAADP-binding sites and TPC1 (Figure 3) raises the question of a functional role of TPCs in mediating acrosome reaction. To address whether NAADP-induced Ca^{2+} mobilization is generally affected upon TPC1 deletion, we stimulated wild-type and TPC1-deficient sperm with *trans*-Ned-19 doses eliciting an increase in intracellular Ca^{2+} (Figure 5C and Supplemental Figure S4B). Figure 6A shows that stimulation of wild-type sperm with 100 µM *trans*-Ned-19 resulted in a fast and transient Ca^{2+} signal. However, in TPC1-null sperm, no difference in the kinetics and magnitude of the response to 100 µM *trans*-Ned-19 was detectable (Figure 6A, TPC1 [–/–] 100 µM Ned19). To test whether *TPCN1* gene deletion generally hampers acrosomal exocytosis, we initially determined spontaneous loss of the acrosomal vesicle in sperm of TPC1-null and wild-type spermatozoa. To evaluate whether TPC1 deletion impairs the acrosomal exocytotic machinery, we quantified the stimulatory effect of direct increase in cytosolic Ca^{2+} on acrosomal loss. We incubated in vitro capacitated sperm in KRB buffer supplemented with 10 mM $CaCl_2$ or 10 mM $CaCl_2$ together with 10 µM Ca^{2+} ionophore A23187 (Kirkman-Brown *et al.*, 2002). As expected, on quantifying the proportion of spontaneous loss of the acrosomal vesicle after 90 min (Figure 6B, 90 min) followed by additional incubation in KRB buffer supplemented with SLO (Figure 6B, 120 min), we found that acrosome reaction rates of sperm of both genotypes constantly increased over time (Nakanishi *et al.*, 2001). However, in calculating statistical differences between spontaneous acrosome reaction rates between sperm of wild-type and TPC1-null sperm, we found no significant differences. The same was true when $CaCl_2$ and $CaCl_2$ supplemented with A23187 were added to both sperm populations. $CaCl_2$ (Figure 6B, Ca^{2+}), as well as $CaCl_2$ plus A23187 (Figure 6B, Ca^{2+} + A23187), led to considerable enhancement of acrosomal secretion rates in sperm of both genotypes compared with spontaneous loss of the acrosomal vesicle upon capacitation. However, average percentages of TPC1-null sperm that had undergone acrosome reaction were not significantly different from those of wild-type sperm (Figure 6B). Because these results imply that the acrosomal machinery in TPC1-deficient germ cells is intact, the potency of NAADP to elicit acrosome reaction was determined in TPC-null sperm. We incubated capacitated spermatozoa of wild-type and TPC-null males with one of the three maximally active NAADP doses (Figure 5, A and B) before quantifying acrosome reaction rates. Data summarized in Figure 6C illustrate that very low (50 nM) and high NAADP doses (50 µM) elicited a strong increase in acrosome reaction rates in TPC1-null mutant sperm, which was not significantly different from the percentage of acrosome reaction rates in wild-type sperm. However, comparing the percentages of acrosome reaction induced upon application of 1 µM NAADP between TPC1-deficient and wild-type sperm revealed an unresponsiveness of TPC1-deficient spermatozoa to low, micromolar NAADP doses (Figure 6C).

DISCUSSION

Phylogenetically preserved role of NAADP in fertilization

Given studies on different species of echinodermata, which represent traditional model organisms with which to study principles of reproduction (Neill and Vacquier, 2004), and results from our present study on fertilization in mammals, we postulate a phylogenetically preserved role of NAADP in triggering acrosome reaction. This ranges from animals with external fertilization to animals that fertilize internally. In sea urchins, contact of sperm with glycoproteins of the egg jelly layer—the physiological signal for sperm to undergo acrosome reaction (Trimmer and Vacquier, 1986)—elicits a rapid and transient elevation in the concentration of intracellular NAADP (Churchill *et al.*, 2003), which might be synthesized by a Ca^{2+}-regulated NAADP synthase (Vasudevan *et al.*, 2008). In addition, based on use of vesicular fractions of spermatozoa that represent a mixture of acrosomal vesicles and resealed plasma membranes, NAADP was found to promote an increase in intravesicular Ca^{2+} (Vasudevan *et al.*, 2010). Our results presented here document for the first time that physiological NAADP concentrations can trigger fusion of the acrosomal vesicle in mouse spermatozoa (Figure 5, A and B) and that *Zona pellucida*–induced acrosome reaction is blocked by the NAADP antagonist *trans*-Ned-19 (Figure 5E). NAADP-mediated fusion of lysosome-related organelles is relevant not only for male germ cells but also for the oocyte: Ca^{2+}-regulated exocytosis of acidic dense-core granules of sea urchin eggs, which also represent functional homologues of endo/lysosomes (McNeil *et al.*, 2000), were indeed the first lysosome-related organelles in which the

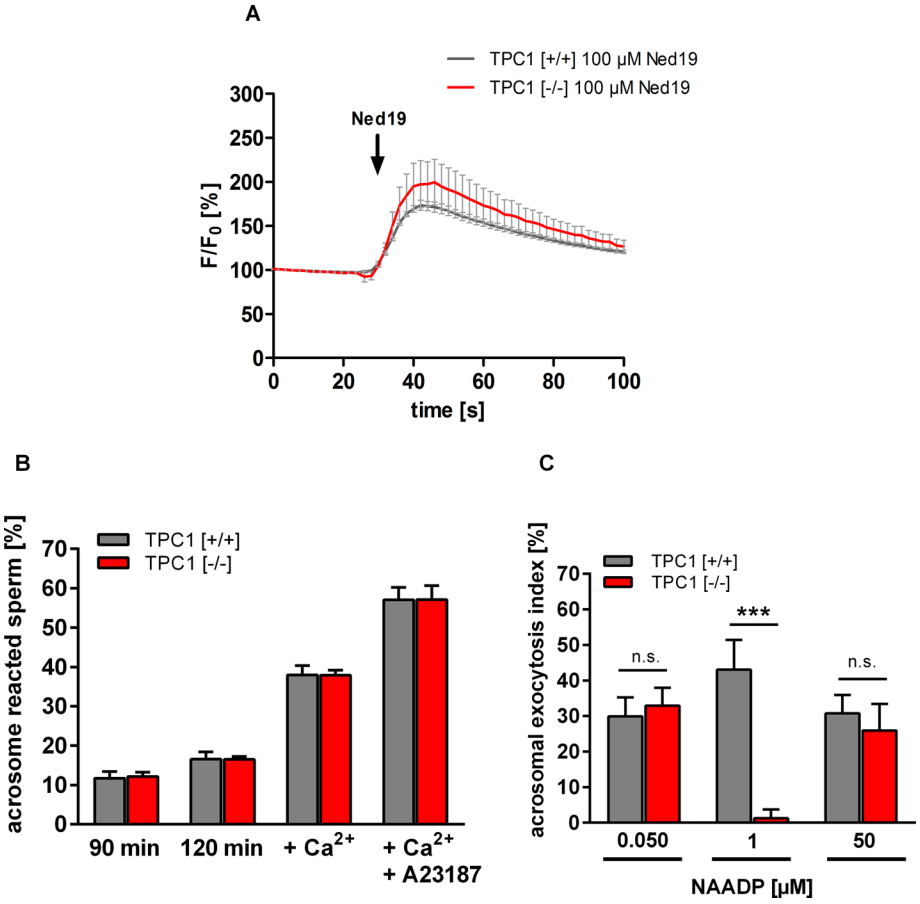

FIGURE 6: Comparison of *trans*-Ned-19–induced Ca^{2+} increase and acrosome reaction rates in TPC1-deficient and wild-type sperm. (A) Time course of *trans*-Ned-19–induced increase in $[Ca^{2+}]_i$ in TPC1 wild-type and TPC1-deficient sperm. To compare directly the effect of *TPCN1* gene deletion on *trans*-Ned-19–induced increase in $[Ca^{2+}]_i$, capacitated wild-type [+/+] and TPC1-null sperm [–/–] were loaded with the Ca^{2+} fluorescent dye Fluo8-AM (10 µM). Fluorescence intensity was determined at the excitation wavelength of Fluo8-AM (485 nm) using a yellow fluorescent protein filter and a microscope-based imaging system. After a 30-s baseline interval to determine the Fluo8 fluorescence intensity in the head region of adhered sperm, 100 µM *trans*-Ned-19 was added. Note that sperm of both genotypes responded with a comparable transient increase in $[Ca^{2+}]_i$ to stimulation with *trans*-Ned-19. Fluorescence intensity, recorded in 2-s intervals, was normalized to the initial values of each single cell and is presented as percentage of basal Fluo8 emission (F/F_0). Data show mean values ± SEM of sperm preparations of three TPC1 wild-type and knockout animals (total number of measured sperm, 14–35 cells/animal). (B) Comparison of spontaneous acrosome reaction rates of TPC1-deficient and wild-type spermatozoa. Spontaneous loss of the acrosomal vesicle was quantified via incubation of spermatozoa of wild-type and TPC1-deficient animals for either 90 min in capacitation buffer or KRB buffer supplemented with SLO (120 min). In addition, permeabilized sperm were treated with 10 mM $CaCl_2$ (Ca^{2+}) or 10 mM $CaCl_2$ together with 10 µM of the Ca^{2+} ionophore A23187 (Ca^{2+} + A23187). $CaCl_2$, as well as $CaCl_2$ plus A23187, markedly increased acrosomal secretion rates in sperm of both genotypes when compared with the basic level of spontaneously acrosome-reacted spermatozoa ([+/+], 16.58 ± 1.81%; [–/–], 16.58 ± 0.68%). However, in calculating statistical differences between acrosome reaction rates between sperm of both genotypes, no significant differences ($p \leq 0.05$) were detected. (C) NAADP-induced acrosome reaction in sperm of TPC1-null mice compared with wild-type spermatozoa. Capacitated and permeabilized epididymal sperm of TPC1-knockout and wild-type animals were stimulated with NAADP, and acrosome reaction rates were determined. Because dose-dependent relationship analyses show three response peaks for NAADP, NAADP doses inducing maximal acrosomal secretion rates were applied (50 nM, 1 µM, 50 µM). Quantification of the acrosomal status of treated sperm revealed that very low (50 nM) and high NAADP doses (50 µM) elicited strong increase in acrosome reaction rates in TPC1-null sperm, which was not significantly different from the percentage of acrosome reaction in wild-type sperm. However, comparing the elevation in the percentage of acrosome reaction induced upon application of 1 µM NAADP wild-type sperm shows the expected increase in acrosome reaction rate. In contrast, TPC1-deficient spermatozoa did not show responsiveness to this NAADP concentration. Data presented as acrosomal exocytosis index are mean values ± SEM of independent experiments with different mouse sperm preparations ([+/+], $n = 10$; [–/–], $n = 9$). Statistical analysis was done using an unpaired Student's *t* test comparing the acrosomal exocytosis index of sperm of both genotypes. ***$p < 0.001$; n.s., not significant.

Ca^{2+}-mobilizing ability of NAADP was discovered (Churchill *et al.*, 2002). However, the second messenger NAADP seems to play an important role in the process of final gamete fusion. A small "trigger bolus" of NAADP (Morgan, 2011) generated in sperm upon egg contact may be transferred to the egg and thereby contribute to the characteristic cortical Ca^{2+} flash reaction (Lim *et al.*, 2001; Churchill *et al.*, 2003; Moccia *et al.*, 2006), essential to prevent polyspermic fertilization (Jaffe, 1976). Regarding these critical functions of NAADP during the sequential process of fertilization, we speculate that defects in NAADP-controlled cellular reactions may result in reduced fecundity or even infertility. It is worth mentioning that sperm of Niemann–Pick type C1 (NPC1)–deficient mice, a metabolic disorder characterized by reduction in lysosomal Ca^{2+} storage capacity (Lloyd-Evans *et al.*, 2008; Karten *et al.*, 2009), are unable to fuse with a mature egg (Fan *et al.*, 2006; Butler *et al.*, 2007). Whether infertility of NPC1-knockout mice is de facto the result of a dysfunction in NAADP-promoted "acidic Ca^{2+} store mobilization" (Patel and Docampo, 2010) in germ cells or whether sterility is a consequence of abnormal cholesterol accumulation in the late endocytic pathway described for other cells (Rosenbaum and Maxfield, 2011) needs to be examined in future studies.

Functional significance of NAADP in driving acrosome reaction

One of the characteristic features of the acrosome reaction is that fusion between the outer acrosomal membrane and the facing plasma membrane occurs at multiple loci (Barros *et al.*, 1967; Harper *et al.*, 2008). This is particularly important for spermatozoa, as complete fusion of the acrosomal vesicle not only allows the entire release of digestive enzymes, but also ensures exposure of the whole inner acrosomal membrane to enable fusion with the oocyte's plasma membrane. However, the regulatory relationship between the zipper-like fenestration of the two membranes and the release of acrosomal Ca^{2+}, essential for final fusion pore formation (De Blas *et al.*, 2002; Herrick *et al.*, 2005), has only been partially defined. The results of the present study

show for the first time that NAADP is inducing acrosome reaction at physiological concentrations and without any additional extracellular Ca^{2+}. Furthermore, maximal percentages of NAADP-induced secretion rates (Figure 5A) were in the same range as those directly induced by the acrosomal Ca^{2+} inducer Rab3A (Yunes *et al.*, 2000; De Blas *et al.*, 2005). Remarkably, the IP_3-R antagonist 2-APB attenuated NAADP-induced acrosome reactions (Supplemental Figure S5C). Moreover, colocalization of IP_3-R and TPC1 in detergent-resistant lipid raft platforms (Supplemental Figure S6) was observed. These lipid rafts embody a membrane-organizing principle of spatial sequestration, which leads to a subcellular concentration of components of the secretory machinery at the "acrosomal synapse" (Zitranski *et al.*, 2010), the posterior region of the sperm head (Gadella *et al.*, 2008; Nixon and Aitken, 2009; Zitranski *et al.*, 2010). Thus it is tempting to speculate that the "trigger hypothesis" postulated for NAADP (Churchill and Galione, 2001; Patel *et al.*, 2011) also controls acrosomal secretion. Sensitization of adjacent IP_3-R may subsequently promote greater Ca^{2+} efflux from the acrosomal vesicle, followed by formation of fusion pores at multiple sites. However, direct experimental evidence that NAADP is indeed inducing release of acrosomal Ca^{2+}, essential to achieve activation of IP_3-R, is lacking (for review see Rossi *et al.*, 2012). Initial experimental approaches in which we stimulated spermatozoa with the membrane-permeable NAADP-AM did not lead to detectable changes in intracellular calcium concentration ($[Ca^{2+}]_i$). This might be due to the extreme instability of NAADP-AM in aqueous solutions (Parkesh *et al.*, 2008). Another possible explanation is that NAADP-promoted responses in sperm are very small and spatially restricted, as described for TPC1 (for review see Zhu *et al.*, 2010b; Galione *et al.*, 2011). Moreover, depletion of the acidic acrosomal Ca^{2+} store with the vacuolar H^+-ATPase inhibitor bafilomycin (Drose and Altendorf, 1997) is not possible because bafilomycin treatment already elicits a loss of the acrosome (unpublished data), even in Ca^{2+}-free media (Nakanishi *et al.*, 2001). Thus future studies are necessary to clarify whether NAADP is indeed able to mobilize Ca^{2+} from the lysosome-related acrosomal vesicle.

Relationship between TPCs and NAADP

Our finding that NAADP is able to drive acrosomal secretion raises the important question of the molecular identity of channel proteins that functionally link the second messenger NAADP to acrosomal exocytosis. Although there is accumulating evidence that TPCs do not directly bind NAADP but require specific, yet-unidentified "mediator" proteins (Lin-Moshier *et al.*, 2012; Walseth *et al.*, 2012), they have been suggested to represent molecular targets of NAADP (for review see Galione *et al.*, 2011; Hooper and Patel, 2012). The present study shows that NAADP-binding sites and TPC1 colocalize at the acrosomal Ca^{2+} store (Figures 2 and 3). Furthermore, NAADP-triggered acrosome reaction reflects typical properties described for TPC proteins (for review see Galione *et al.*, 2009; Hooper and Patel, 2012). 1) Registered responses were not detected for its chemical analogue NADP (Figure 5, A and B) and 2) were blocked by its antagonist *trans*-Ned-19 (Figure 5D). In addition, 3) NAADP-induced acrosomal secretion was already detectable when applying NAADP doses quantified upon ligand stimulation (Churchill *et al.*, 2003; Masgrau *et al.*, 2003; Yamasaki *et al.*, 2005; Gasser *et al.*, 2006; Lewis *et al.*, 2012; Schmid *et al.*, 2012). 4) Acrosomal secretion shows typical self-inactivation properties at higher NAADP doses (Aarhus *et al.*, 1996). Remarkably, on comparing acrosomal secretion rates induced by physiological intracellular NAADP concentrations, two-well-defined and nonoverlapping U-shaped response curves were apparent (Figure 5, A and B, 50 nM, 1 µM). Furthermore, acrosome reaction induced by low, micromolar NAADP concentrations was completely absent in sperm of TPC1-deficient mice (Figure 6C). This confirms our suggestion that two independent NAADP pathways are functionally operative in triggering acrosomal secretion. Because responses at nanomolar NAADP doses are not affected upon *TPCN1* gene deletion, one might suggest that the registered moderate reproductive phenotype of the TPC1-knockout mouse strain may in part be due to a functional compensation of other NAADP targets. In this context it is important to note that TPC2 shows maximal responses at an intracellular NAADP concentration of ~30 nM (Calcraft *et al.*, 2009; Zong *et al.*, 2009; Galione *et al.*, 2011). One may speculate that TPC2 could be the corresponding molecular NAADP target, as the high-affinity NAADP pathway triggering acrosomal secretion peaks at ~50 nM NAADP (Figure 5A), and transcripts for TPC2 are present in reproductive tissue (Supplemental Figure S1). We currently cannot exclude that other NAADP-sensitive channels residing in membranes of acidic lysosome-related organelles are operative in controlling acrosomal secretion (for review see Kilfoil *et al.*, 2009; Sumoza-Toledo and Penner, 2011; Guse, 2012). However, TPC2-knockout mice are also characterized by a subtle phenotype (Calcraft *et al.*, 2009). Thus we suggest a high degree of functional redundancy for TPC subtypes and/or other mediators of Ca^{2+} signaling (Zhu *et al.*, 2010b), which might be important to ensure success of fertilization. Therefore it will be interesting to characterize the reproductive phenotypes of mice carrying a targeted gene deletion for both TPCN1 and TPCN2. However, the observation that the same second messenger at different concentrations elicits activation of different molecular targets, which in the end converge on the same cellular response, may also be important to ensure fusion of the large acrosomal vesicle. In sea urchin spermatozoa, egg-contact-induced increase in NAADP is characterized by rapid (2 min) and very transient kinetics (Churchill *et al.*, 2003), a phenomenon characteristic of NAADP-dependent responses (Aley *et al.*, 2013). Owing to possible rapid catabolic inactivation of NAADP (Billington *et al.*, 2004) and reduction in the local NAADP concentration by diffusion, it is apparent that egg-induced NAADP increase at the tip of the acrosomal cap rapidly decreases (Buffone *et al.*, 2009), leading to low local NAADP concentration at the posterior region of the acrosome. To ensure robust NAADP-evoked response over the entire acrosomal area, NAADP targets with extremely high affinities for NAADP are of functional importance. However, whether the two NAADP-gated targets triggering acrosome reaction are indeed essential to precisely adjust local NAADP concentration to an activation of adjacent acrosomal IP_3-R and whether this mechanism is also operative in other cellular systems where NAADP controls regulated exocytosis (for review see Galione, 2011; Hooper and Patel, 2012) need to be explored in future studies.

MATERIALS AND METHODS

Animal and human studies

All experiments comply with *Principles of Animal Care*, publication no. 85-23, revised 1985, of the National Institutes of Health and with the current laws of Germany.

Human semen samples were obtained by masturbation from healthy volunteers with written informed consent and used in anonymous form. According to current German laws, no further approval was necessary for noninvasive recovery of samples from volunteers.

Animals and antibodies

Male adult mice (C57BL/6 and BALB/c) and rats (Wistar) were raised at the Ludwig-Maximilians-University of Munich (Munich, Germany)

and kept at a 12-h light/dark cycle with food and water ad libitum; mice were kept in an individually ventilated cage system provided by Techniplast (Hohenpeissenberg, Germany). Mice with a gene-targeted deletion of TPCN1 were constructed by excision of exon 3 of the *TPCN1* gene sequence using the Cre-loxP recombination system (N.K., unpublished data) and were bred on a mixed (129SV and C57BL/6) background (backcrossed to C57BL/6 in third generation). Littermate wild-type animals or animals with identical genetic background and age were used as control as indicated for each set of experiment.

To identify TPC1 and TPC2 in mouse and rat spermatozoa, we used the following antibodies: a polyclonal rabbit anti-TPC1 antibody recognizing a synthetic peptide from the C-terminal region of mouse TPC1 (ab80961; Abcam, Cambridge, United Kingdom), as well as a polyclonal goat anti-TPC1 raised against an epitope mapping the C-terminus of TPC1 of human origin, which was also suggested to recognize TPC1 of mouse and rat (sc-67973; Santa Cruz, Biotechnology, Heidelberg, Germany). In addition, an affinity purified rabbit anti-TPC1 specific antibody, named TPC1NK, was used which was generated against a C-terminal epitope of the murine TPC1 protein (J.C. and N.K., unpublished data). To identify the TPC2 protein, two different antisera, each generated against a mouse-derived synthetic peptide specific for the cytoplasmic domain of TPC2, were used (ab81101, Abcam; ABIN351016, antibodies-online, Aachen, Germany). To test for the specificity of TPC-specific antisera, we explored antigenic peptides used to generate subtype-specific anti-TPC antibodies. To this end, antisera were pretreated with 10-fold excess of the corresponding immunogenic peptide; efficiency of neutralization was then tested in immunohistochemical and immunocytochemical analyses performed as described (Meyer *et al.*, 2012) or in Western blot analyses (Ackermann *et al.*, 2008). In addition, specifications of the applied anti-TPC1 antibodies were expanded by examining respective tissues (kidney, testis, epididymis, spermatozoa) from the TPC1-knockout mouse line.

Streptolysine O permeabilization and acrosome reaction assay

SLO plasma membrane permeabilization of mouse spermatozoa was accomplished as described previously (De Blas *et al.*, 2005; Hutt *et al.*, 2005; Ackermann *et al.*, 2009). Briefly, capacitated spermatozoa (90 min) diluted to (5–10) $\times$ 10^6 sperm/ml were permeabilized for 30 min at 37°C in modified Krebs–Ringer bicarbonate buffer (KRB; 5.6 mM glucose, 0.55 mM sodium pyruvate, 25 mM Na_2HCO_3, 53 mM sodium lactate, 99.6 mM NaCl, 4.8 mM KCl, 1.2 mM K_2HPO_4, 1.2 mM $MgSO_4$; pH 7.4), supplemented with 5 U/ml SLO (KRB/SLO). Because sperm permeabilization allows free access of the purine nucleotides into the sperm's cytosol (Branham *et al.*, 2006; Diaz *et al.*, 1996), calculated NAADP and NADP concentrations during the process of sperm permeabilization correspond to intracellular purine nucleotide concentrations. Aliquots of 100 mM stock solutions of either NAADP or NADP (diluted in double-distilled water and stored at –20°C) were thawed on ice. Before full sperm capacitation, appropriate predilutions were prepared in KRB/SLO buffer, thoroughly mixed, and used to make KRB/SLO buffer solutions with a 10-fold higher NAADP/NADP concentration than intended for sperm stimulation. Subsequently, a 20-µl aliquot of each puridine nucleotide solution was mixed with 180 µl of the sperm suspension, also diluted in KRB/SLO, and sperm were incubated for 30 min at 37°C. Of importance, stock solutions and predilutions of puridine nucleotides were thawed only once. Moreover, to ensure proper sperm permeabilization, elevation of acrosomal secretion of each sperm preparation was determined after increasing extracellular calcium to 10 mM; results for which the rate of acrosome reaction induced by high extracellular $CaCl_2$ was not >10% were not included. As negative controls, uncapacitated as well as nonpermeabilized sperm were assessed for NAADP responsiveness. Under both conditions, NAADP at different concentrations did not elicit significant elevation in acrosomal secretion rate (Supplemental Material and Tables 1 and 2).

To analyze the effect of the RyR antagonist ruthenium red RR (Ozawa, 2010) and the IP_3-R inhibitor 2-APB (Bootman *et al.*, 2002) on NAADP-induced acrosome reaction, capacitated sperm diluted in KRB/SLO buffer were pretreated for 15 min at 37°C with the different modulators, and subsequently KRB/SLO solution supplemented with NAADP was added and sperm were incubated for an additional 30 min at 37°C. *Trans*-Ned-19 was directly diluted in KRB/SLO buffer with no preincubation time. Analysis of acrosome reaction rates of wild-type and TPC1-deficient animals was performed with littermates and cousins. To determine the rate of spontaneous loss of the acrosomal vesicle, cell samples of permeabilized sperm were incubated with the KRB/SLO solution only. The reaction was stopped by fixation of the germ cells (20 mM Na_2HPO_4, 150 mM NaCl, 7.5% formaldehyde) for at least 30 min. Subsequently sperm were washed with a postfixation buffer (100 mM ammonium acetate, pH 9.0) and air dried on glass slides. Acrosome-reacted sperm were determined using the Coomassie brilliant blue (G-250) staining method (Zeginiadou *et al.*, 2000; Meyer *et al.*, 2012). For each incubation condition, at least 200 spermatozoa were scored on blinded slides using an Olympus CKX 31microscope (Olympus, Hamburg, Germany) equipped with bright-field light optics. Subsequently, the percentage of spermatozoa without acrosome was calculated. Data are either presented as absolute percentage of acrosome-reacted sperm or expressed as acrosomal exocytosis index (Ackermann *et al.*, 2008). Data of each experiment were normalized by subtracting the rate of spontaneous loss of the acrosomal vesicle after capacitation (90 min) and subsequently calculated as percentage of the acrosome reaction rate observed in the positive control (10 mM $CaCl_2$).

Induction of acrosome reaction with *Zona pellucida*

Zona pellucida-induced acrosome reaction in mouse spermatozoa was performed as described (Meyer *et al.*, 2012). Briefly, freshly prepared ovaries from 20 adult female mice were homogenized in 2 ml of HB buffer (150 mM NaCl, 25 mM triethanolamine, 1 mM $MgCl_2$, 1 mM $CaCl_2$, pH 8.5, supplemented with proteinase inhibitor, 1 mM phenylmethylsulfonyl fluoride, 0.02% [wt/vol] aprotinin, and 0.02% [wt/vol] DNase). After addition of Nonidet-P40 and sodium deoxycholate (1% in HB buffer) and further homogenization, the homogenate was fractionated on a three-step Percoll gradient (2/10/22% in HB buffer). After centrifugation at 200 $\times$ *g* and 4°C for 2 h (Eppendorf A-4-44, swing-out rotor), the "10% Percoll fraction" containing *Zona pellucida* was collected and diluted with 40 ml HB buffer; subsequently *Zona pellucida* was concentrated by centrifugation (16,000 $\times$ *g*, 10 min, 4°C). After an additional wash with 1.5 ml of HB buffer the pellet was resuspended in 200 µl of HB buffer, and an aliquot was used to count the number of *Zona pellucida* ghosts. For extraction of soluble ZP glycoproteins, HB buffer used to solve the pure zonae was shifted to 2.5 (37% HCl) and heated for 15 min at 37°C; subsequently, nonsolubilized material was separated by centrifugation (16,000 $\times$ *g*, 10 min). After neutralization of the collected supernatant with 5 M NaOH, solubilized zonae and a buffer control treated in the same way were frozen in aliquots and stored at –70°C until use. To induce acrosome reaction, sperm were capacitated for 90 min and diluted to a concentration of ~3 $\times$ 10^6 spermatozoa/ml KRB; subsequently 50 µl of the sperm suspension was incubated for

30 min at 37°C with solubilized zonae (10 zonae/µl). As a negative control, samples were incubated with the corresponding control buffer used for heat solubilization (see earlier description). After *Zona pellucida* stimulation, sperm were fixed, washed, air-dried on glass slides, and assessed for acrosomal status as described.

Fluorescence-based acrosomal staining methods

The fluorescence properties of the NAADP antagonist *trans*-Ned-19 permit visualization of NAADP-binding sites in intact cells (Naylor *et al.*, 2009). To uncover NAADP receptor–binding sites in intact spermatozoa, capacitated epididymal mouse sperm, resuspended in HS buffer supplemented with 15 mM $NaHCO_3$, were incubated for 1 h at 37°C in the dark with 100 µM *trans*-Ned-19 (Naylor *et al.*, 2009). To monitor possible autofluorescence of sperm cells at the characteristic *trans*-Ned-19 excitation/emission properties (355/415 nm), an aliquot of capacitated sperm was incubated in buffer alone. Subsequently, sperm cells were transferred to slides, covered with coverslips and directly imaged for *trans*-Ned-19 fluorescence using a DAPI-filter set (IX 71; Olympus).

To selectively label the acidic acrosome in living sperm, the membrane-permeable fluorescent dye LysoTracker Red (Wubbolts *et al.*, 1996; Magez *et al.*, 1997) was used as described previously (Sun-Wada *et al.*, 2002). Briefly, capacitated mouse spermatozoa were incubated for 30 min at 37°C with 75 nM LysoTracker Red DND-99 (Invitrogen, Darmstadt, Germany) and washed twice with HS buffer supplemented with 15 mM $NaHCO_3$ (centrifugation, 400 × *g*, 5 min); subsequently, fluorescence distribution was monitored using a rhodamine filter (IX 71; Olympus). For acrosomal PNA staining (Aviles *et al.*, 1997), cells fixed with acetone/methanol (1:1, –20°C, 10 min) were incubated with fluorescein isothiocyanate (FITC)–coupled PNA diluted in 10% fetal calf serum/phosphate-buffered saline (PBS) for 30 min at room temperature in the dark. After removal of excess fluorescence-conjugated lectin by three washes with PBS, samples were coated with fluorescent mounting medium (DakoCytomation, Hamburg, Germany) and assessed for acrosomal status using an Olympus IX 71 microscope.

Immunoelectron microscopy

Immunoelectron microscopic analyses were essentially performed as described (Neesen *et al.*, 2002). Briefly, mouse testes samples of TPC1 wild-type and TPC1-knockout animals were immersion fixed for 2 h in a fixative consisting of 2% paraformaldehyde and 0.05% glutaraldehyde in 0.05 M sodium cacodylate buffer (0.1 M, pH 7.3). Samples were washed with sodium cacodylate buffer, dehydrated in ethanol and propylene oxide as described (Neesen *et al.*, 2002), and embedded in LR Gold Resin. Ultrathin sections were cut on a Reichert ultramicrotome equipped with a diamond knife and mounted on 100-mesh gold grids. Grids were incubated with the anti-TPC1NK antibody (6.6 µg/ml), diluted in Tris-buffered saline (TBS; 10 mM Tris/HCl, pH 8.0, 150 mM NaCl) for 12 h at 4°C, washed with TBS three times for 15 min and, incubated with a 1:100 dilution of a goat anti-rabbit IgG conjugated to colloidal 10-nm gold particles (BBInternational, Cardiff, United Kingdom). Then sections were washed again with TBS, briefly treated with alkaline lead citrate and uranyl acetate solutions, and examined in an electron microscope (Tecnai12BT; FEI, Hillsboro, OR).

Evaluation of reproductive performance and analysis of reproductive organs and spermatozoa of TPC1-knockout mice

Wild-type, heterozygous, and homozygous TPC1 mice of similar ages were bred in a continuous monogamous mating system and analyzed for average litter size, including surviving and dead pups, and time needed to litter. Statistical analysis was done by comparing obtained genotype distribution of offspring pups (homozygous, [–/–]; heterozygous, [+/–]; wild-type [+/+]) to the expected Mendelian ratio using the chi-squared test with two degrees of freedom. Departure from expectation was considered statistically significant when $p < 0.05$. To assess gonad weight, mice were killed by cervical dislocation and weighed to determine total body weight. Reproductive tissues were dissected, and testes weighed immediately after dissection. To determine the number of mature sperm, epididymides of individual animals were transferred to 2 ml of HS buffer supplemented with 15 mM $NaHCO_3$/0.5% BSA and cut several times with a sharp scalpel. After a swim-out time of at least 15 min at 37°C, sperm were collected, diluted 1:40 (vol/vol) in water, and counted in a Neubauer chamber (Brand, Wertheim, Germany). Morphometric analysis of reproductive organs and spermatozoa of wild-type and TPC1-null sperm was performed as described (Meyer *et al.*, 2012).

Statistical analysis

Unless stated otherwise, statistical analyses were performed using the Student's *t* test. Results with a calculated $p < 0.05$ were considered to be significant. Levels of statistical significance are indicated by $*p < 0.05$, $**p < 0.01$, and $***p < 0.001$.

ACKNOWLEDGMENTS

We thank Heinz-Gerhard Janser for excellent technical assistance. We also thank Gerhard Aumüller (Department of Anatomy and Cell Biology, University of Marburg, Marburg, Germany) and Artur Mayerhofer (Institute for Cell Biology, LMU Munich, Munich, Germany) for help with the histological analyses of testis morphology, Nele Zitranski (Walther-Straub-Institute of Pharmacology and Toxicology, LMU Munich) for advice on isolating lipid rafts, and Uwe Schulte (Institute of Physiology, University of Freiburg, Freiburg, Germany) for helpful discussion. Financial support was provided in part by Jürgen Solinski (Walther-Straub-Institute of Pharmacology and Toxicology, LMU Munich) for his support by creating the images, the Hertie-Exzellenzprogramm Neurowissenschaften, the Deutsche Forschungsgemeinschaft (BO 1668/5-1; KL 1119/4-1; WA2597), and the SME innovation program ZIM of the German Federal Ministry of Economics and Technology (BMWi). The funders had no role in study design, data collection and analysis, decision to publish, or preparation of the manuscript.

REFERENCES

Aarhus R, Dickey DM, Graeff RM, Gee KR, Walseth TF, Lee HC (1996). Activation and inactivation of Ca2+ release by NAADP+. J Biol Chem 271, 8513–8516.

Abou-Haila A, Tulsiani DR (2009). Signal transduction pathways that regulate sperm capacitation and the acrosome reaction. Arch Biochem Biophys 485, 72–81.

Ackermann F, Zitranski N, Borth H, Buech T, Gudermann T, Boekhoff I (2009). CaMKIIalpha interacts with multi-PDZ domain protein MUPP1 in spermatozoa and prevents spontaneous acrosomal exocytosis. J Cell Sci 122, 4547–4557.

Ackermann F, Zitranski N, Heydecke D, Wilhelm B, Gudermann T, Boekhoff I (2008). The multi-PDZ domain protein MUPP1 as a lipid raft-associated scaffolding protein controlling the acrosome reaction in mammalian spermatozoa. J Cell Physiol 214, 757–768.

Aley PK, Singh N, Brailoiu GC, Brailoiu E, Churchill GC (2013). Nicotinic acid adenine dinucleotide phosphate (NAADP) is a second messenger in muscarinic receptor-induced contraction of guinea pig trachea. J Biol Chem 288, 10986–10993.

Andersson H, Baechi T, Hoechl M, Richter C (1998). Autofluorescence of living cells. J Microsc 191, 1–7.

Arredouani A, Evans AM, Ma J, Parrington J, Zhu MX, Galione A (2010). An emerging role for NAADP-mediated Ca2+ signaling in the pancreatic beta-cell. Islets 2, 323–330.
Ashton JC (2011). Knockout controls and the specificity of cannabinoid CB2 receptor antibodies. Br J Pharmacol 163, 1113.
Aviles M, Castells MT, Martinez-Menarguez JA, Abascal I, Ballesta J (1997). Localization of penultimate carbohydrate residues in zona pellucida and acrosomes by means of lectin cytochemistry and enzymatic treatments. Histochem J 29, 583–592.
Barros C, Bedford JM, Franklin LE, Austin CR (1967). Membrane vesiculation as a feature of the mammalian acrosome reaction. J Cell Biol 34, C1–C5.
Bedu-Addo K, Costello S, Harper C, Machado-Oliveira G, Lefievre L, Ford C, Barratt C, Publicover S (2008). Mobilisation of stored calcium in the neck region of human sperm–a mechanism for regulation of flagellar activity. Int J Dev Biol 52, 615–626.
Bello OD, Zanetti MN, Mayorga LS, Michaut MA (2012). RIM, Munc13, and Rab3A interplay in acrosomal exocytosis. Exp Cell Res 318, 478–488.
Berg I, Potter BV, Mayr GW, Guse AH (2000). Nicotinic acid adenine dinucleotide phosphate (NAADP(+)) is an essential regulator of T-lymphocyte Ca(2+)-signaling. J Cell Biol 150, 581–588.
Berridge MJ (2002). The endoplasmic reticulum: a multifunctional signaling organelle. Cell Calcium 32, 235–249.
Billington RA, Thuring JW, Conway SJ, Packman L, Holmes AB, Genazzani AA (2004). Production and characterization of reduced NAADP (nicotinic acid-adenine dinucleotide phosphate). Biochem J 378, 275–280.
Bootman MD, Collins TJ, Mackenzie L, Roderick HL, Berridge MJ, Peppiatt CM (2002). 2-Aminoethoxydiphenyl borate (2-APB) is a reliable blocker of store-operated Ca2+ entry but an inconsistent inhibitor of InsP3-induced Ca2+ release. FASEB J 16, 1145–1150.
Bowman EJ, Siebers A, Altendorf K (1988). Bafilomycins: a class of inhibitors of membrane ATPases from microorganisms, animal cells, and plant cells. Proc Natl Acad Sci USA 85, 7972–7976.
Brailoiu E *et al.* (2009). Essential requirement for two-pore channel 1 in NAADP-mediated calcium signaling. J Cell Biol 186, 201–209.
Brailoiu E, Hooper R, Cai X, Brailoiu GC, Keebler MV, Dun NJ, Marchant JS, Patel S (2010). An ancestral deuterostome family of two-pore channels mediates nicotinic acid adenine dinucleotide phosphate-dependent calcium release from acidic organelles. J Biol Chem 285, 2897–2901.
Branham MT, Mayorga LS, Tomes CN (2006). Calcium-induced acrosomal exocytosis requires cAMP acting through a protein kinase A-independent, Epac-mediated pathway. J Biol Chem 281, 8656–8666.
Buffone MG, Rodriguez-Miranda E, Storey BT, Gerton GL (2009). Acrosomal exocytosis of mouse sperm progresses in a consistent direction in response to zona pellucida. J Cell Physiol 220, 611–620.
Butler A, Gordon RE, Gatt S, Schuchman EH (2007). Sperm abnormalities in heterozygous acid sphingomyelinase knockout mice reveal a novel approach for the prevention of genetic diseases. Am J Pathol 170, 2077–2088.
Calcraft PJ *et al.* (2009). NAADP mobilizes calcium from acidic organelles through two-pore channels. Nature 459, 596–600.
Cancela JM, Churchill GC, Galione A (1999). Coordination of agonist-induced Ca2+-signalling patterns by NAADP in pancreatic acinar cells. Nature 398, 74–76.
Chu DS, Shakes DC (2012). Spermatogenesis. Adv Exp Med Biol 757, 171–203.
Churchill GC, Galione A (2000). Spatial control of Ca2+ signaling by nicotinic acid adenine dinucleotide phosphate diffusion and gradients. J Biol Chem 275, 38687–38692.
Churchill GC, Galione A (2001). Prolonged inactivation of nicotinic acid adenine dinucleotide phosphate-induced Ca2+ release mediates a spatiotemporal Ca2+ memory. J Biol Chem 276, 11223–11225.
Churchill GC, Okada Y, Thomas JM, Genazzani AA, Patel S, Galione A (2002). NAADP mobilizes Ca(2+) from reserve granules, lysosome-related organelles, in sea urchin eggs. Cell 111, 703–708.
Churchill GC, O'Neill JS, Masgrau R, Patel S, Thomas JM, Genazzani AA, Galione A (2003). Sperm deliver a new second messenger: NAADP. Curr Biol 13, 125–128.
Costello S, Michelangeli F, Nash K, Lefievre L, Morris J, Machado-Oliveira G, Barratt C, Kirkman-Brown J, Publicover S (2009). Ca2+-stores in sperm: their identities and functions. Reproduction 138, 425–437.
Darszon A, Nishigaki T, Beltran C, Trevino CL (2011). Calcium channels in the development, maturation, and function of spermatozoa. Physiol Rev 91, 1305–1355.
Davis LC *et al.* (2012). NAADP activates two-pore channels on T cell cytolytic granules to stimulate exocytosis and killing. Curr Biol 22, 2331–2337.
De Blas G, Michaut M, Trevino CL, Tomes CN, Yunes R, Darszon A, Mayorga LS (2002). The intraacrosomal calcium pool plays a direct role in acrosomal exocytosis. J Biol Chem 277, 49326–49331.
De Blas GA, Roggero CM, Tomes CN, Mayorga LS (2005). Dynamics of SNARE assembly and disassembly during sperm acrosomal exocytosis. PLoS Biol 3, e323.
Dell'Angelica EC, Mullins C, Caplan S, Bonifacino JS (2000). Lysosome-related organelles. FASEB J 14, 1265–1278.
Diaz A, Dominguez L, Fornes MW, Burgos MH, Mayorga LS (1996). Acrosome content release in streptolysin O permeabilized mouse spermatozoa. Andrologia 28, 21–26.
Drose S, Altendorf K (1997). Bafilomycins and concanamycins as inhibitors of V-ATPases and P-ATPases. J Exp Biol 200, 1–8.
Fan J, Akabane H, Graham SN, Richardson LL, Zhu GZ (2006). Sperm defects in mice lacking a functional Niemann-Pick C1 protein. Mol Reprod Dev 73, 1284–1291.
Florman HM, Jungnickel MK, Sutton KA (2008). Regulating the acrosome reaction. Int J Dev Biol 52, 503–510.
Gadella BM, Tsai PS, Boerke A, Brewis IA (2008). Sperm head membrane reorganisation during capacitation. Int J Dev Biol 52, 473–480.
Galione A (2011). NAADP receptors. Cold Spring Harb Perspect Biol 3, a004036.
Galione A, Chuang KT (2012). Pyridine nucleotide metabolites and calcium release from intracellular stores. Adv Exp Med Biol 740, 305–323.
Galione A, Evans AM, Ma J, Parrington J, Arredouani A, Cheng X, Zhu MX (2009). The acid test: the discovery of two-pore channels (TPCs) as NAADP-gated endolysosomal Ca(2+) release channels. Pflugers Arch 458, 869–876.
Galione A, Parrington J, Funnell T (2011). Physiological roles of NAADP-mediated Ca2+ signaling. Sci China Life Sci 54, 725–732.
Galione A, Ruas M (2005). NAADP receptors. Cell Calcium 38, 273–280.
Gasser A, Bruhn S, Guse AH (2006). Second messenger function of nicotinic acid adenine dinucleotide phosphate revealed by an improved enzymatic cycling assay. J Biol Chem 281, 16906–16913.
Genazzani AA, Empson RM, Galione A (1996). Unique inactivation properties of NAADP-sensitive Ca2+ release. J Biol Chem 271, 11599–11602.
Guse AH (2012). Linking NAADP to ion channel activity: a unifying hypothesis. Sci Signaling 5, pe18.
Harper CV, Barratt CL, Publicover SJ (2004). Stimulation of human spermatozoa with progesterone gradients to simulate approach to the oocyte. Induction of [Ca(2+)](i) oscillations and cyclical transitions in flagellar beating. J Biol Chem 279, 46315–46325.
Harper CV, Cummerson JA, White MR, Publicover SJ, Johnson PM (2008). Dynamic resolution of acrosomal exocytosis in human sperm. J Cell Sci 121, 2130–2135.
Hartree EF (1975). The acrosome-lysosome relationship. J Reprod Fertil 44, 125–126.
Herkenham M, Rathore P, Brown P, Listwak SJ (2011). Cautionary notes on the use of NF-kappaB p65 and p50 antibodies for CNS studies. J Neuroinflammation 8, 141.
Herrick SB, Schweissinger DL, Kim SW, Bayan KR, Mann S, Cardullo RA (2005). The acrosomal vesicle of mouse sperm is a calcium store. J Cell Physiol 202, 663–671.
Ho HC, Suarez SS (2001). An inositol 1,4,5-trisphosphate receptor-gated intracellular Ca(2+) store is involved in regulating sperm hyperactivated motility. Biol Reprod 65, 1606–1615.
Ho HC, Suarez SS (2003). Characterization of the intracellular calcium store at the base of the sperm flagellum that regulates hyperactivated motility. Biol Reprod 68, 1590–1596.
Hooper R, Patel S (2012). NAADP on target. Adv Exp Med Biol 740, 325–347.
Hutt DM, Baltz JM, Ngsee JK (2005). Synaptotagmin VI and VIII and syntaxin 2 are essential for the mouse sperm acrosome reaction. J Biol Chem 280, 20197–20203.
Ishibashi K, Suzuki M, Imai M (2000). Molecular cloning of a novel form (two-repeat) protein related to voltage-gated sodium and calcium channels. Biochem Biophys Res Commun 270, 370–376.
Jaffe LA (1976). Fast block to polyspermy in sea urchin eggs is electrically mediated. Nature 261, 68–71.
Jahn R, Fasshauer D (2012). Molecular machines governing exocytosis of synaptic vesicles. Nature 490, 201–207.
Johnson LR, Moss SB, Gerton GL (1999). Maintenance of motility in mouse sperm permeabilized with streptolysin O. Biol Reprod 60, 683–690.

Karten B, Peake KB, Vance JE (2009). Mechanisms and consequences of impaired lipid trafficking in Niemann-Pick type C1-deficient mammalian cells. Biochim Biophys Acta 1791, 659–670.
Kilfoil PJ, Tipparaju SM, Barski OA, Bhatnagar A (2009). Regulation of ion channels by pyridine nucleotides. Circ Res 112, 721–741.
Kirkman-Brown JC, Punt EL, Barratt CL, Publicover SJ (2002). Zona pellucida and progesterone-induced Ca2+ signaling and acrosome reaction in human spermatozoa. J Androl 23, 306–315.
Kuroda Y, Kaneko S, Yoshimura Y, Nozawa S, Mikoshiba K (1999). Are there inositol 1,4,5-triphosphate (IP3) receptors in human sperm? Life Sci 65, 135–143.
Langa F *et al.* (2003). Generation and phenotypic analysis of sigma receptor type I (sigma 1) knockout mice. Eur J Neurosci 18, 2188–2196.
Lee HC (2001). Physiological functions of cyclic ADP-ribose and NAADP as calcium messengers. Ann Rev Pharmacol Toxicol 41, 317–345.
Lefievre L, Chen Y, Conner SJ, Scott JL, Publicover SJ, Ford WC, Barratt CL (2007). Human spermatozoa contain multiple targets for protein S-nitrosylation: an alternative mechanism of the modulation of sperm function by nitric oxide. Proteomics 7, 3066–3084.
Lewis AM *et al.* (2012). beta-Adrenergic receptor signaling increases NAADP and cADPR levels in the heart. Biochem Biophys Res Commun 427, 326–329.
Lim D, Kyozuka K, Gragnaniello G, Carafoli E, Santella L (2001). NAADP+ initiates the Ca2+ response during fertilization of starfish oocytes. FASEB J 15, 2257–2267.
Lin-Moshier Y, Walseth TF, Churamani D, Davidson SM, Slama JT, Hooper R, Brailoiu E, Patel S, Marchant JS (2012). Photoaffinity labeling of nicotinic acid adenine dinucleotide phosphate (NAADP) targets in mammalian cells. J Biol Chem 287, 2296–2307.
Lloyd-Evans E, Morgan AJ, He X, Smith DA, Elliot-Smith E, Sillence DJ, Churchill GC, Schuchman EH, Galione A, Platt FM (2008). Niemann-Pick disease type C1 is a sphingosine storage disease that causes deregulation of lysosomal calcium. Nat Med 14, 1247–1255.
Magez S, Geuskens M, Beschin A, del Favero H, Verschueren H, Lucas R, Pays E, de Baetselier P (1997). Specific uptake of tumor necrosis factor-alpha is involved in growth control of *Trypanosoma brucei*. J Cell Biol 137, 715–727.
Maruyama T, Kanaji T, Nakade S, Kanno T, Mikoshiba K (1997). 2APB, 2-aminoethoxydiphenyl borate, a membrane-penetrable modulator of Ins(1,4,5)P3-induced Ca2+ release. J Biochem 122, 498–505.
Masgrau R, Churchill GC, Morgan AJ, Ashcroft SJ, Galione A (2003). NAADP: a new second messenger for glucose-induced Ca2+ responses in clonal pancreatic beta cells. Curr Biol 13, 247–251.
Maximov A, Tang J, Yang X, Pang ZP, Sudhof TC (2009). Complexin controls the force transfer from SNARE complexes to membranes in fusion. Science 323, 516–521.
Mayorga LS, Tomes CN, Belmonte SA (2007). Acrosomal exocytosis, a special type of regulated secretion. IUBMB Life 59, 286–292.
McNeil PL, Vogel SS, Miyake K, Terasaki M (2000). Patching plasma membrane disruptions with cytoplasmic membrane. J Cell Sci 113 (Pt 11) 1891–1902.
Meizel S, Deamer DW (1978). The pH of the hamster sperm acrosome. J Histochem Cytochem 26, 98–105.
Meyer D *et al.* (2012). Expression of tas1 taste receptors in mammalian spermatozoa: functional role of tas1r1 in regulating Basal ca and cAMP concentrations in spermatozoa. PLoS One 7, e32354.
Meyvis TK, De Smedt SC, Van Oostveldt P, Demeester J (1999). Fluorescence recovery after photobleaching: a versatile tool for mobility and interaction measurements in pharmaceutical research. Pharm Res 16, 1153–1162.
Moccia F, Nusco GA, Lim D, Kyozuka K, Santella L (2006). NAADP and InsP3 play distinct roles at fertilization in starfish oocytes. Dev Biol 294, 24–38.
Montoliu L (2012). Mendel: a simple Excel workbook to compare the observed and expected distributions of genotypes/phenotypes in transgenic and knockout mouse crosses involving up to three unlinked loci by means of a chi2 test. Transgenic Res 21, 677–681.
Moreno RD, Ramalho-Santos J, Chan EK, Wessel GM, Schatten G (2000). The Golgi apparatus segregates from the lysosomal/acrosomal vesicle during rhesus spermiogenesis: structural alterations. Dev Biol 219, 334–349.
Morgan AJ (2011). Sea urchin eggs in the acid reign. Cell Calcium 50, 147–156.
Naaby-Hansen S *et al.* (2001). Co-localization of the inositol 1,4,5-trisphosphate receptor and calreticulin in the equatorial segment and in membrane bounded vesicles in the cytoplasmic droplet of human spermatozoa. Mol Hum Reprod 7, 923–933.
Nakanishi T, Ikawa M, Yamada S, Toshimori K, Okabe M (2001). Alkalinization of acrosome measured by GFP as a pH indicator and its relation to sperm capacitation. Dev Biol 237, 222–231.
Naylor E *et al.* (2009). Identification of a chemical probe for NAADP by virtual screening. Nat Chem Biol 5, 220–226.
Neesen J, Hartwich T, Brandhorst G, Aumuller G, Glaser B, Burfeind P, Mendoza-Lujambio I (2002). Tep22, a novel testicular expressed gene, is involved in the biogenesis of the acrosome and the midpiece of the sperm tail. Biochem Biophys Res Commun 297, 737–748.
Neill AT, Vacquier VD (2004). Ligands and receptors mediating signal transduction in sea urchin spermatozoa. Reproduction 127, 141–149.
Nixon B, Aitken RJ (2009). The biological significance of detergent-resistant membranes in spermatozoa. J Reprod Immunol 83, 8–13.
Olson SD, Fauci LJ, Suarez SS (2011). Mathematical modeling of calcium signaling during sperm hyperactivation. Mol Hum Reprod 17, 500–510.
Ozawa T (2010). Modulation of ryanodine receptor Ca2+ channels (review). Mol Med Rep 3, 199–204.
Parkesh R *et al.* (2008). Cell-permeant NAADP: a novel chemical tool enabling the study of Ca2+ signalling in intact cells. Cell Calcium 43, 531–538.
Parton RG (1996). Caveolae and caveolins. Curr Opin Cell Biol 8, 542–548.
Patel S, Docampo R (2010). Acidic calcium stores open for business: expanding the potential for intracellular Ca2+ signaling. Trends Cell Biol 20, 277–286.
Patel S, Ramakrishnan L, Rahman T, Hamdoun A, Marchant JS, Taylor CW, Brailoiu E (2011). The endo-lysosomal system as an NAADP-sensitive acidic Ca(2+) store: role for the two-pore channels. Cell Calcium 50, 157–167.
Pitt SJ *et al.* (2010). TPC2 is a novel NAADP-sensitive Ca2+ release channel, operating as a dual sensor of luminal pH and Ca2+. J Biol Chem 285, 35039–35046.
Rahman T, Taylor CW (2009). Dynamic regulation of IP3 receptor clustering and activity by IP3. Channels (Austin) 3, 226–232.
Rizo J, Sudhof TC (2012). The membrane fusion enigma: SNAREs, Sec1/Munc18 proteins, and their accomplices—guilty as charged? Annu Rev Cell Dev Biol 28, 279–308.
Rosen D *et al.* (2009). Analogues of the nicotinic acid adenine dinucleotide phosphate (NAADP) antagonist Ned-19 indicate two binding sites on the NAADP receptor. J Biol Chem 284, 34930–34934.
Rosenbaum AI, Maxfield FR (2011). Niemann-Pick type C disease: molecular mechanisms and potential therapeutic approaches. J Neurochem 116, 789–795.
Rossato M, Di Virgilio F, Rizzuto R, Galeazzi C, Foresta C (2001). Intracellular calcium store depletion and acrosome reaction in human spermatozoa: role of calcium and plasma membrane potential. Mol Hum Reprod 7, 119–128.
Rossi AM, Tovey SC, Rahman T, Prole DL, Taylor CW (2012). Analysis of IP3 receptors in and out of cells. Biochim Biophys Acta 1820, 1214–1227.
Rothberg KG, Heuser JE, Donzell WC, Ying YS, Glenney JR, Anderson RG (1992). Caveolin, a protein component of caveolae membrane coats. Cell 68, 673–682.
Ruas M *et al.* (2010). Purified TPC isoforms form NAADP receptors with distinct roles for Ca(2+) signaling and endolysosomal trafficking. Curr Biol 20, 703–709.
Schmid F, Bruhn S, Weber K, Mittrucker HW, Guse AH (2011). CD38: a NAADP degrading enzyme. FEBS Lett 585, 3544–3548.
Schmid F, Fliegert R, Westphal T, Bauche A, Guse AH (2012). Nicotinic acid adenine dinucleotide phosphate (NAADP) degradation by alkaline phosphatase. J Biol Chem 287, 32525–32534.
Sumoza-Toledo A, Penner R (2011). TRPM2: a multifunctional ion channel for calcium signalling. J Physiol 589, 1515–1525.
Sun-Wada GH, Imai-Senga Y, Yamamoto A, Murata Y, Hirata T, Wada Y, Futai M (2002). A proton pump ATPase with testis-specific E1-subunit isoform required for acrosome acidification. J Biol Chem 277, 18098–18105.
Sutton KA, Jungnickel MK, Florman HM (2008). A polycystin-1 controls postcopulatory reproductive selection in mice. Proc Natl Acad Sci USA 105, 8661–8666.
Tapia R, Velasco I (1997). Ruthenium red as a tool to study calcium channels, neuronal death and the function of neural pathways. Neurochem Int 30, 137–147.
Tomes CN (2007). Molecular mechanisms of membrane fusion during acrosomal exocytosis. Soc Reprod Fertil Suppl 65, 275–291.
Trevino CL, Santi CM, Beltran C, Hernandez-Cruz A, Darszon A, Lomeli H (1998). Localisation of inositol trisphosphate and ryanodine receptors

during mouse spermatogenesis: possible functional implications. Zygote 6, 159–172.
Trimmer JS, Vacquier VD (1986). Activation of sea urchin gametes. Ann Rev Cell Biol 2, 1–26.
Tsai PS, Brewis IA, van Maaren J, Gadella BM (2012). Involvement of complexin 2 in docking, locking and unlocking of different SNARE complexes during sperm capacitation and induced acrosomal exocytosis. PLoS One 7, e32603.
Tsai PS, Garcia-Gil N, van Haeften T, Gadella BM (2010). How pig sperm prepares to fertilize: stable acrosome docking to the plasma membrane. PLoS One 5, e11204.
Tugba Durlu-Kandilci N, Ruas M, Chuang KT, Brading A, Parrington J, Galione A (2010). TPC2 proteins mediate nicotinic acid adenine dinucleotide phosphate (NAADP)- and agonist-evoked contractions of smooth muscle. J Biol Chem 285, 24925–24932.
Vasudevan SR, Galione A, Churchill GC (2008). Sperm express a Ca2+-regulated NAADP synthase. Biochem J 411, 63–70.
Vasudevan SR, Lewis AM, Chan JW, Machin CL, Sinha D, Galione A, Churchill GC (2010). The calcium-mobilizing messenger nicotinic acid adenine dinucleotide phosphate participates in sperm activation by mediating the acrosome reaction. J Biol Chem 285, 18262–18269.
Visconti PE, Krapf D, de la Vega-Beltran JL, Acevedo JJ, Darszon A (2011). Ion channels, phosphorylation and mammalian sperm capacitation. Asian J Androl 13, 395–405.
Walensky LD, Snyder SH (1995). Inositol 1,4,5-trisphosphate receptors selectively localized to the acrosomes of mammalian sperm. J Cell Biol 130, 857–869.
Walseth TF, Lin-Moshier Y, Jain P, Ruas M, Parrington J, Galione A, Marchant JS, Slama JT (2012). Photoaffinity labeling of high affinity nicotinic acid adenine dinucleotide phosphate (NAADP)-binding proteins in sea urchin egg. J Biol Chem 287, 2308–2315.
Wang X *et al*. (2012). TPC proteins are phosphoinositide- activated sodium-selective ion channels in endosomes and lysosomes. Cell 151, 372–383.
Wassarman PM, Litscher ES (2008). Mammalian fertilization: the eggs multifunctional zona pellucida. Int J Dev Biol 52, 665–676.
Weibull C, Christiansson A (1986). Extraction of proteins and membrane lipids during low temperature embedding of biological material for electron microscopy. J Microsc 142, 79–86.
Wubbolts R, Fernandez-Borja M, Oomen L, Verwoerd D, Janssen H, Calafat J, Tulp A, Dusseljee S, Neefjes J (1996). Direct vesicular transport of MHC class II molecules from lysosomal structures to the cell surface. J Cell Biol 135, 611–622.
Yamasaki M, Thomas JM, Churchill GC, Garnham C, Lewis AM, Cancela JM, Patel S, Galione A (2005). Role of NAADP and cADPR in the induction and maintenance of agonist-evoked Ca2+ spiking in mouse pancreatic acinar cells. Curr Biol 15, 874–878.
Yu FH, Yarov-Yarovoy V, Gutman GA, Catterall WA (2005). Overview of molecular relationships in the voltage-gated ion channel superfamily. Pharmacol Rev 57, 387–395.
Yunes R, Michaut M, Tomes C, Mayorga LS (2000). Rab3A triggers the acrosome reaction in permeabilized human spermatozoa. Biol Reprod 62, 1084–1089.
Zanetti N, Mayorga LS (2009). Acrosomal swelling and membrane docking are required for hybrid vesicle formation during the human sperm acrosome reaction. Biol Reprod 81, 396–405.
Zeginiadou T, Papadimas J, Mantalenakis S (2000). Acrosome reaction: methods for detection and clinical significance. Andrologia 32, 335–343.
Zhang F, Xu M, Han WQ, Li PL (2012). Reconstitution of lysosomal NAADP-TRP-ML1 signaling pathway and its function in TRP-ML1(-/-) cells. Am J Physiol Cell Physiol 301, C421–C430.
Zhu MX, Evans AM, Ma J, Parrington J, Galione A (2010a). Two-pore channels for integrative Ca signaling. Commun Integr Biol 3, 12–17.
Zhu MX, Ma J, Parrington J, Calcraft PJ, Galione A, Evans AM (2010b). Calcium signaling via two-pore channels: local or global, that is the question. Am J Physiol Cell Physiol 298, C430–C441.
Zhu MX, Ma J, Parrington J, Galione A, Evans AM (2010c). TPCs: endolysosomal channels for Ca2+ mobilization from acidic organelles triggered by NAADP. FEBS Lett 584, 1966–1974.
Ziegler BL, Lamping C, Thoma S, Thomas CA (1992). Single-cell cDNA-PCR: removal of contaminating genomic DNA from total RNA using immobilized DNase I. Biotechniques 13, 726–729.
Zitranski N, Borth H, Ackermann F, Meyer D, Viewig L, Breit A, Gudermann T, Boekhoff I (2010). The "acrosomal synapse": subcellular organization by lipid rafts and scaffolding proteins exhibits high similarities in neurons and mammalian spermatozoa. Commun Integr Biol 3, 513–521.
Zong X, Schieder M, Cuny H, Fenske S, Gruner C, Rotzer K, Griesbeck O, Harz H, Biel M, Wahl-Schott C (2009). The two-pore channel TPCN2 mediates NAADP-dependent Ca(2+)-release from lysosomal stores. Pflugers Arch 458, 891–899.